Therapeutic strategies to restore intratumoral immune activity in human cancer

Kaptein, P.

Chapter 4

Addition of interleukin-2 overcomes resistance to neoadjuvant CTLA4 and PD1 blockade in ex vivo patient tumors

Paulien Kaptein[1]†, Celia Jacoberger-Foissac[2]†, Petros Dimitriadis[3]†, Paula Voabil[1], Marjolein de Bruijn[1], Simone Brokamp[1], Irene Reijers[3], Judith Versluis[3], Gahyathiri Nallan[2], Hannah Triscott[2,4], Elizabeth McDonald[2], Joshua Tay[2], Georgina V Long[5,6,7], Christian U Blank[1,3]‡*, Daniela S Thommen[1]‡, Michele WL Teng[2,4]‡

[1] Division of Molecular Oncology and Immunology, The Netherlands Cancer Institute, Amsterdam, The Netherlands, 1066 CX.

[2] QIMR Berghofer Medical Research Institute, Brisbane, Queensland, Australia, 4006.

[3] Department of Medical Oncology, The Netherlands Cancer Institute, Amsterdam, The Netherlands, 1066 CX.

[4] School of Medicine, University of Queensland, Herston, Queensland, Australia, 4006.

[5] Melanoma Institute Australia, The University of Sydney, Sydney, Australia, 2006.

[6] Faculty of Medicine and Health, The University of Sydney, Sydney, Australia, 2006.

[7] Royal North Shore and Mater Hospitals, Sydney, Australia, 2065.

* Corresponding author.

† These authors share first authorship

‡ These authors share senior authorship

Published in Science Translational Medicine, Apr 22 2022, 14(642):eabj9779

Abstract

Neoadjuvant immunotherapy with anti-CTLA4+anti-PD1 monoclonal antibodies (mAbs) has demonstrated remarkable pathological responses and relapse-free survival in ~80% of patients with clinically detectable stage III melanoma. However, about 20% of the treated patients do not respond. In pre-treatment biopsies of patients with melanoma, we found that resistance to neoadjuvant CTLA4+PD1 blockade was associated with a low CD4/IL2 gene signature. Ex vivo, addition of IL2 to CTLA4+PD1 blockade induced T cell activation and deep immunological responses in anti-CTLA4+anti-PD1 resistant human tumor specimens. In the 4T1.2 breast cancer mouse model of neoadjuvant immunotherapy, triple combination of anti-CTLA4+anti-PD1+IL2 cured almost twice as many mice as compared to dual checkpoint inhibitor therapy. This improved efficacy was due to the expansion of tumor-specific CD8+ T cells, and improved pro-inflammatory cytokine polyfunctionality of both CD4+ and CD8+ T effector cells and regulatory T cells. Depletion studies suggested CD4+ T cells were critical for priming of CD8+ T cell immunity against 4T1.2 and helped in the expansion of tumor-specific CD8+ T cells early after neoadjuvant triple immunotherapy. Our results suggest that the addition of IL2 can overcome resistance to neoadjuvant anti-CTLA4+anti-PD1, providing the rationale for testing this combination as a neoadjuvant therapy in patients with early-stage cancer.

Introduction

Neoadjuvant application of immune checkpoint inhibitors (ICIs) is currently the most promising immunotherapy for cancer treatment[1]. This is based on the idea, that in early-stage disease, responses to checkpoint inhibition are more frequent likely due to reduced tumor-mediated immune suppression[2], and that tumor-specific T cell expansion is greater when ICI is administered before, compared to after, complete surgical resection of the tumor. This has been demonstrated pre-clinically using the orthotopic 4T1.2 triple negative breast tumor mouse allograft model, which to date represents the best model where surgery and lethal metastases can be assessed in the context of neoadjuvant versus adjuvant therapy in a robust and timely manner[3]. Clinically, proof-of-concept that neoadjuvant compared to adjuvant immunotherapy is more efficacious was demonstrated in a small trial in patients with melanoma[4]. In early-stage melanoma, several trials have reported 30-33% pathologic response rates (pRR) for neoadjuvant PD1 blockade[5,6] and 71-80% pRR for the combination of neoadjuvant CTLA4+PD1 blockade[7,8]. This high pRR in the combination ICI-treated group is unparalleled and associated with long-term relapse-free survival (RFS)[9]. Amongst the patients who achieved a pathological complete response (pCR) or near pCR, hardly any patients relapsed, suggesting this parameter was a strong surrogate for long-term outcome[9]. First attempts to characterize high-risk stage III patients with melanoma responding to neoadjuvant CTLA4+PD1 blockade identified tumor mutational burden (TMB) and an interferon-gamma (IFNγ) signature to be independent baseline predictors of response[4,10]. Extended human RNA signature analyses have shown that pRR and RFS were also associated with a T cell signature and a Basic leucine zipper transcription factor ATF-like 3 (BATF3)[11,12]. Pre-clinically, using T cell depletion of wild-type mice or Batf3-/- mice bearing 4T1.2 tumors, T cells and Batf3-lineage derived dendritic cells (DCs) were found to be critical for the efficacy of neoadjuvant immunotherapy[3,12]. Overall, these findings are in agreement with neoadjuvant immunotherapy trials in patients with melanoma showing that patients whose tumors produce low amounts of IFNγ and are TMB low or display a low T cell and BATF3 signature are likely to not respond[4,10,12]. Hence, this raises the question of whether alternative or additional therapy to neoadjuvant CTLA4+PD1 blockade could convert non-responders into responders.

The effective priming of a cytotoxic T cell response is dependent on $CD4^+$ T helper 1 (TH1) cells which increase DC antigen-presentation and co-stimulatory capacity[13]. Activated CD4 TH1 cells are a major source of interleukin 2 (IL2), which has known pro-activation and proliferative functions on T cells[14]. IL2 also improves the chemotactic responsiveness of T cells[15] and was recently shown in mice and humans to induce DC expansion and activation through cytokines produced by IL2-activated T cells[16]. Although the addition of IL2 in combination with other immunotherapies has demonstrated utility in mouse models of cancer mimicking advanced disease and in small clinical trials to treat late-stage disease[17-19], it is unclear whether the use of IL2 in the neoadjuvant setting will also be beneficial. Here in this study, we assessed whether resistance to neoadjuvant CTLA4+PD1

blockade was associated with a low CD4/IL2 signature, whether this impaired response was reversed by the addition of IL2, and whether addition of IL2 further improved the outcome of neoadjuvant dual checkpoint inhibition.

Results

A CD4/IL2 gene signature is associated with response to neoadjuvant ipilimumab + nivolumab

To investigate a potential association between the presence of $CD4^+$ T cells, IL2 and neoadjuvant treatment response, we generated a CD4/IL2 gene expression signature consisting of ten well-known $CD4^+$ T cell-associated genes (*IL2, CD4, ICOS, EOMES, IL21R, IL2RA, IL2RB, IL2RG, CD48*). We performed an analysis of pre-treatment tumor biopsies from patients with stage III melanoma from the PRADO extension cohort (n=79), in which patients were treated with 2 courses of ipilimumab (anti-CTLA4, 1 mg/kg) + nivolumab (anti-PD1, 3 mg/kg) (NCT02977052) (**table S1**). Using this cohort as our training data set, we found that a high CD4/IL2 gene signature was associated with pathological response (53/79, 67%) as defined using the International Neoadjuvant Melanoma Consortium (INMC) response assessment criteria[20]. Using the upper tertile of the CD4/IL2 signature scores as threshold, we found the majority of patients 25/27 (93%) with a high CD4/IL2 signature score responded to neoadjuvant combination immunotherapy (**Fig. 1**). In contrast, for the two-thirds of patients below the threshold and thus defined as having a low CD4/IL2 signature score, only 28/52 (54%) patients responded (**Fig. 1**). We next validated the CD4/IL2 signature score using Nanostring data from an additional independent cohort of patients with stage III melanoma treated with neoadjuvant ipilimumab+nivolumab (OpACIN-neo, n=64) (**table S2**)[7]. Again, we found that the majority of patients 19/21 (90%) with a high CD4/IL2 signature responded to neoadjuvant immunotherapy, whereas only 28/43 (65%) of patients responded with a low CD4/IL2 signature score (**fig. S1A**). Previously, we have shown that both a T cell signature and a BATF3 signature correlated with response to neoadjuvant immunotherapy[4,12]. To compare the CD4/IL2 signature to the T cell and BATF3 signatures, we analyzed the CD8 signature[21] and, as the Nanostring pan-cancer panel used in this study does not include all of the genes, a panel of subset genes from the BATF3 signature[22]. We found that the CD4/IL2 signature correlated with these other signatures (**Fig. 1**, indicated on top, and **fig. S1, B and C**), suggesting that non-response to neoadjuvant immunotherapy might relate to a defect at the stage of early immune activation.

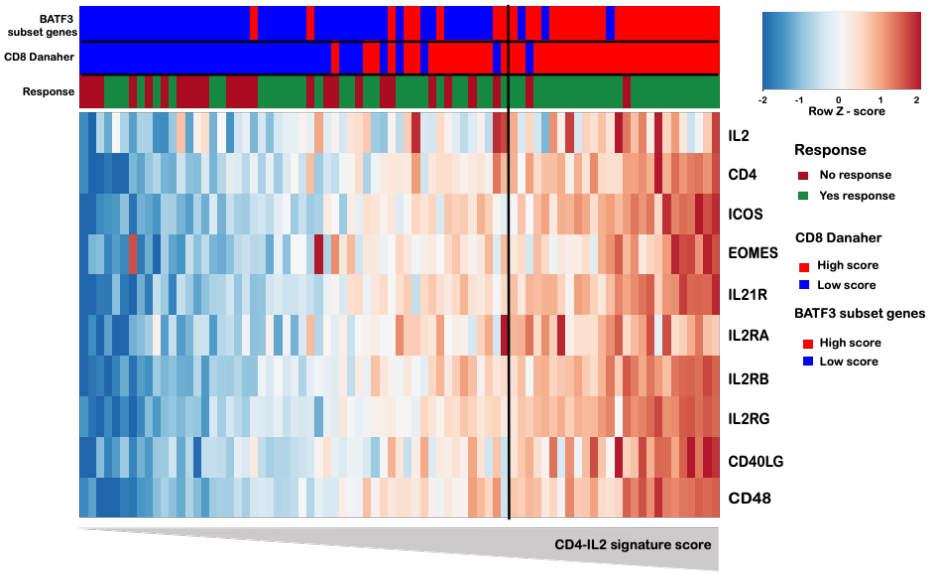

Figure 1. A CD4/IL2 gene signature is associated with response to neoadjuvant ipilimumab + nivolumab. Nanostring data of pre-treatment lymph node tumor biopsies of melanoma patients treated with neoadjuvant ipilimumab+nivolumab in the PRADO study (n=79). The heatmap of the CD4/IL2 gene signature is ordered according to the average expression of the CD4/IL2 gene signature per patient. Each column displays one patient (green: pathologic response, dark red: no pathologic response, blue: low BATF3/CD8 signature score, light red: high BATF3/CD8 signature score). The scores of the BATF3/CD8 signatures are calculated based on the average z-score of *IRF8*, *THBD*, *XCR1* and *CD8A*, *CD8B* respectively. The optimal high-low cutoff is determined by the sROC curves [44] for each signature individually using both PRADO and OpACIN neo patient data (n=143). The rows in the heatmap represents the z-score of the normalized gene expressions. Positive values (red) imply higher gene expression and negative values (blue) indicate lower gene expression. The threshold to define a high CD4/IL2 score is indicated by the vertical black line.

Addition of IL2 to combination checkpoint blockade induces immunological responses in human tumor explants resistant to anti-CTLA4+anti-PD1

To examine the potential benefit of adding IL2 to CTLA4+PD1 blockade, we tested this triple combination therapy in our ex vivo tumor fragment model. We previously have shown that addition of anti-PD1 mAbs to patient-derived tumor fragments (PDTFs) induces T cell activation and early immunological responses that can predict clinical response to PD1 blockade[23]. In this PDTF platform, human tumor tissue obtained from surgical resections or biopsies is cultured whereas the tumor's architecture and its microenvironment are maintained. In addition, therapy-induced changes upon ex vivo immunotherapy treatment can be profiled. To assess whether IL2 treatment had an additive effect to CTLA4+PD1 blockade, we profiled the ex vivo responses of PDTFs from nine human tumor resections that included melanoma (MEL), non-small cell lung cancer (LU), renal cell carcinoma (RE) and ovarian carcinoma (OV) (**Fig. 2A and table S3**). These PDTFs were treated for 48

hours with either the dual combination of anti-CTLA4+anti-PD1 or the triple combination therapy of anti-CTLA4+anti-PD1+IL2 (**Fig. 2A**). Untreated fragments were used as a control for each culture. We assessed first whether anti-CTLA4+anti-PD1±IL2 had an impact on T cell activation by quantifying the expression of the activation markers OX40 and CD137 on $CD8^+$ T cells, $FOXP3^-$ $CD4^+$ T cells, and $FOXP3^+$ $CD4^+$ T cells (**Fig. 2, B and C**). Although dual checkpoint blockade infrequently induced activation of CD8+ T cells in PDTFs as compared to untreated tumor fragments, the effect on both FOXP3- and $FOXP3^+$ $CD4^+$ T cells was insignificant. In contrast, the triple combination therapy induced activation of all three subsets and had the largest effect on $FOXP3^+$ $CD4^+$ T cells, in line with a previously described effect of IL2 on the activation of regulatory T cells (Tregs)[24-26]. Importantly, anti-CTLA4+anti-PD1+IL2 also induced an increase in both the percentage and expression of FOXP3, which was not observed after anti-CTLA4+anti-PD1 treatment (**Fig. 2D**). Thus, within the $CD4^+$ T cell subset, the triple compared to dual combination therapy seemed to mainly cause a shift from $FOXP3^-OX40^-$ to $FOXP3^+OX40^+$ cells (**Fig. 2, E and F**), suggesting that the triple combination therapy promotes the induction of activated $FOXP3^+$ T cells.

To understand whether this increase in activated $FOXP3^+$ T cells induced by the triple combination therapy related to an immune-activating or immunosuppressive response, we next examined 11 cytokines and 13 chemokines secreted by the PDTFs in an extended cohort of 16 tumors during steady-state in untreated control cultures and in response to dual or triple combination immunotherapy (**Fig. 2A, and 3 and table S3**). We first performed unsupervised hierarchical clustering of the cytokines and chemokines produced by PDTFs treated with dual checkpoint blockade compared to untreated PDTFs to identify ex vivo responders to CTLA4+PD1 blockade. We found the dual combination therapy induced changes in cytokine and chemokine secretion patterns in 4/16 (25%) tumors that we defined as anti-CTLA4+anti-PD1 responders, whereas 12/16 (75%) of the tumors displayed only minor treatment-induced changes (anti-CTLA4+anti-PD1 non-responder) (**Fig. 3A and fig. S2A**). Next, we assessed responses to the triple combination-treated therapy condition within these two groups. Strikingly, the triple combination therapy converted 7/12 (58%) of the tumors that were anti- CTLA4+anti-PD1 non-responder into responder (anti-CTLA4+anti-PD1+IL2 responder) (**Fig. 3B and fig. S2B**). In the anti-CTLA4+anti-PD1 responder group, addition of IL2 did not increase cytokine and chemokine secretion further (**Fig. 3B and fig. S2B**). Despite the induction of activated $FOXP3^+$ T cells by the triple combination therapy, which may potentially include Tregs (**Fig. 2, E and F**), the induced immunological response was not suppressive, but led to an increased IFN-γ and TNF-α secretion (**Fig. 3, A and B**). Overall, the response pattern induced by the triple combination therapy was comparable to the response elicited by the dual combination therapy (**Fig. 3C**). Although the non-responding tumors showed a trend towards lower immune infiltration, particularly when compared to anti-CTLA4+anti-PD1+IL2 responders ($p=0.09$), the composition of the infiltrate showed no significant differences between the groups (**Fig. 3D and fig. S3, A and B**).

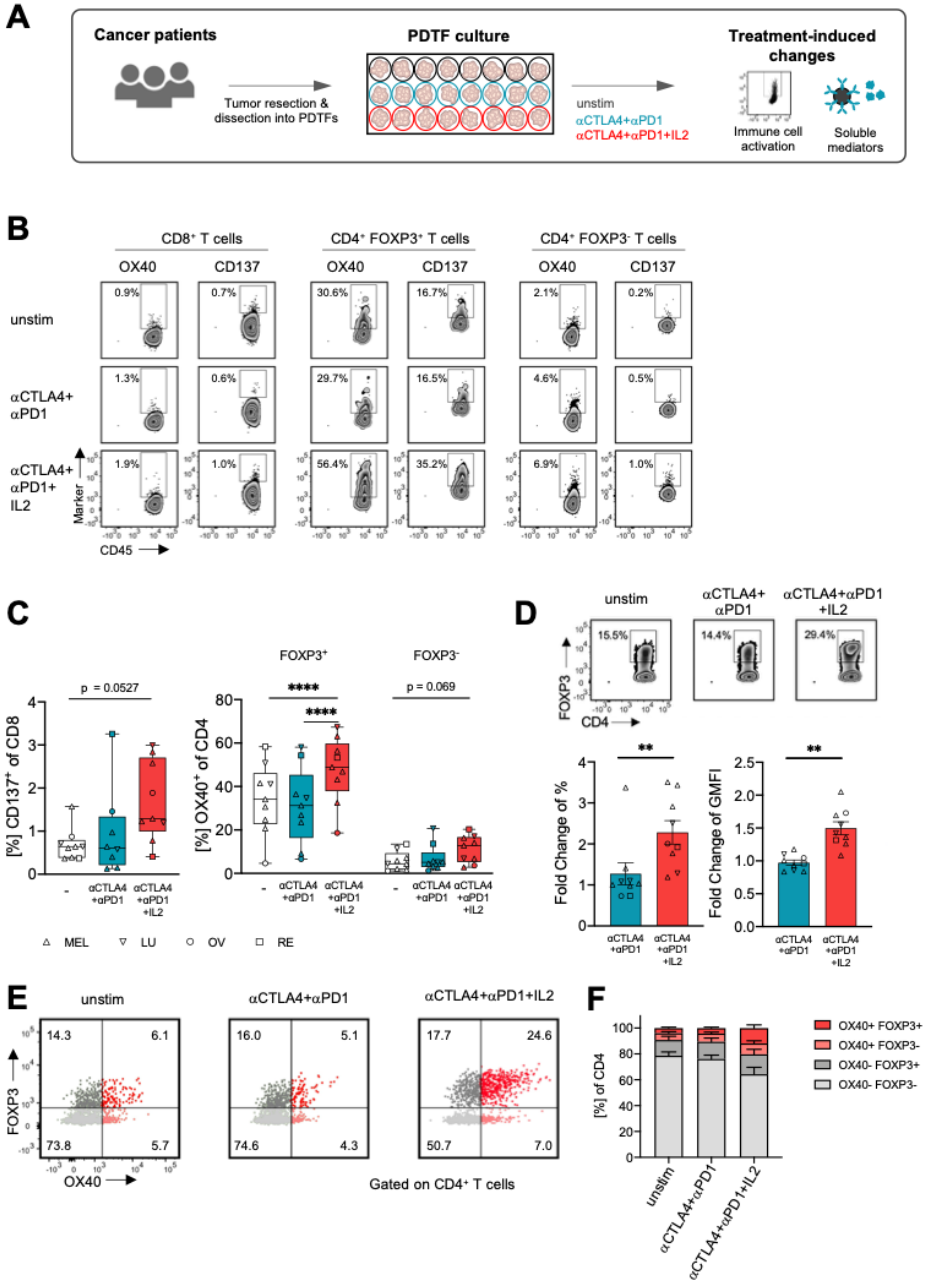

Figure 2. Activation of distinct T cell subsets upon addition of IL2 to *ex vivo* CTLA4+PD1 blockade in resected tumors derived from cancer patients. (A) Experimental overview of the patient-derived tumor fragment (PDTF) platform. **(B-C)** Expression of T cell activation markers in untreated, anti(αCTLA4+αPD1 and αCTLA4+ αPD1+IL2 treated $CD8^+$ T cells, and $CD4^+FOXP3^-$ and $FOXP3^+$ T cells measured by flow cytometry (n=9 tumors). Symbols indicate tumor type (MEL = melanoma, LU = non-small cell lung cancer, OV = overarian carcinoma and RE = renal cell

carcinoma). **(D)** Flow plots showing FOXP3 expression and fold change of FOXP3 percentage and geometric MFI (GMFI) in αCTLA4+αPD1 and αCTLA4+ αPD1+IL2 treated CD4⁺ T cells compared to untreated CD4⁺ T cells. **(E-F)** Expression and quantification of OX40 and FOXP3 in untreated, αCTLA4+ αPD1 and αCTLA4+αPD1+IL2 treated CD4⁺ T cells. Significant differences between groups were determined by Kruskal-Wallis test (**C**) or Mann-Whitney test (**D**). **P<0.01, ****P<0.0001.

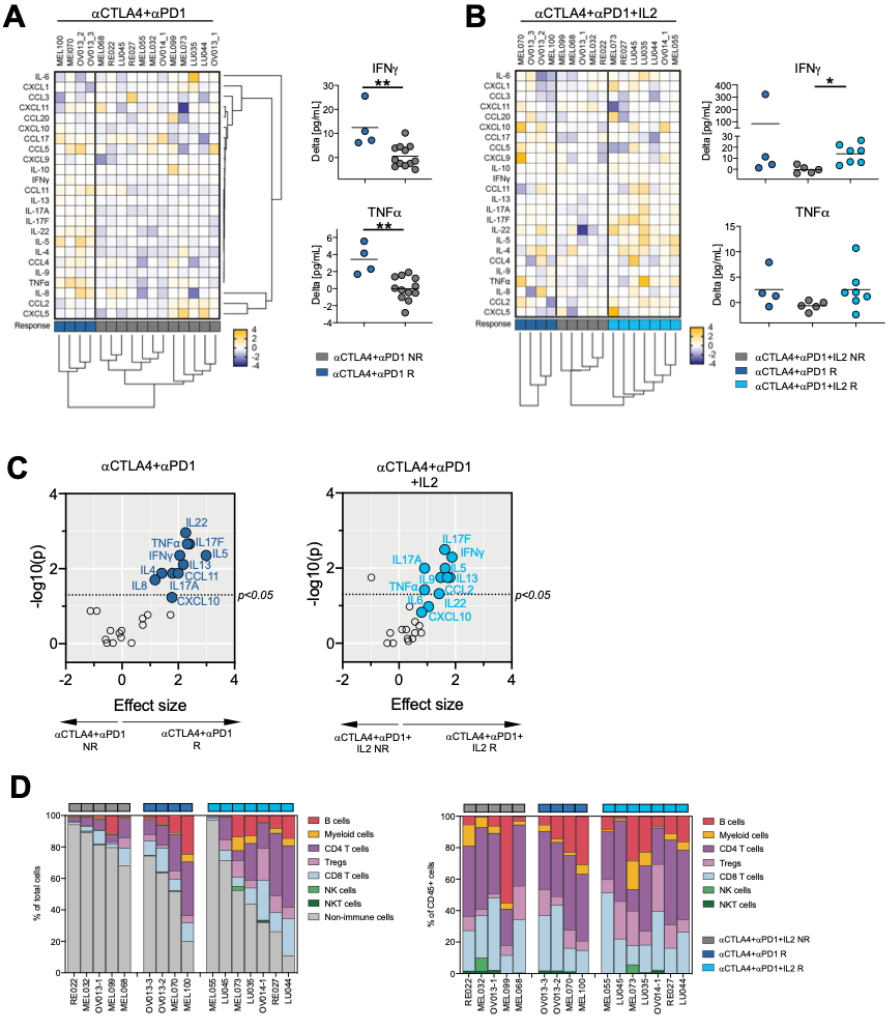

Figure 3. Addition of IL2 induces immunological responses in tumors that are non-responsive to anti-CTLA4+anti-PD1 therapy. (A) Heatmap displaying the normalized delta values between the untreated and anti-CTLA+anti-PD1 conditions for each parameter (11 cytokines and 13 chemokines, n=16 tumors) (left panel). Unsupervised clustering identified two groups of tumors: anti(α)CTLA4+ αPD1 responders (R) and αCTLA4+ αPD1 non-responders (NR). Changes in IFN-γ and TNF-α secretion within the two response groups are displayed in the right panel. **(B)** Heatmap showing the normalized delta values between the untreated and αCTLA4+ αPD1+IL2 treated conditions for the same parameters as in (**A**) (left panel). Supervised clustering identified two subgroups within the

αCTLA4+αPD1 NR group: αCTLA4+αPD1+IL2 R and αCTLA4+ αPD1+IL2 NR tumors. Changes in IFN-γ and TNF-α secretion within the two response groups are displayed in the right panel. **(C)** Correlation between effect sizes (calculated as Hedge's g) and *p* values of normalized changes for all parameters assessed in the αCTLA4+ αPD1 and αCTLA4+αPD1+IL2 treatment groups. **(D)** Quantification of immune cell subsets assessed by flow cytometry within total live cells (left) and total CD45$^+$ immune cells (right). Significant differences between groups were determined by Mann-Whitney test (**A**) or Kruskal-Wallis test (**B**). *P<0.05, **P<0.01.

Addition of IL2 to neoadjuvant anti-CTLA4+anti-PD1 cures tumor-bearing mice

To confirm our ex vivo findings in an in vivo setting, we next tested the addition of IL2 to dual checkpoint inhibition using the spontaneously metastatic triple negative breast cancer model 4T1.2[3]. Previously, we have demonstrated in our neoadjuvant 4T1.2 tumor model, that early expansion of peripheral tumor-specific CD8+ T cells after neoadjuvant immunotherapy strongly correlated with long-term survival[3]. Therefore, we now investigated how the addition of IL2 impacted the efficacy of neoadjuvant anti-CTLA4+anti-PD1 (**Fig. 4**). Groups of mice were treated with the indicated therapy on days 8 and 10 after 4T1.2 mammary fat pad inoculation, followed by surgery on day 13 (**Fig. 4A**). Overall, the triple combination therapy (5/7) compared to the dual combination therapy (3/10) cured a greater proportion of mice, although all treatments either prolonged survival post-surgery or conferred long-term survival benefits compared to the control Ig treated group (**Fig. 4A**). 4T1.2 like many murine cancer cell lines express the envelope glycoprotein (gp70) encoded by the murine leukemia virus (MuLV). Gp70 in the tumor only functions as a neoantigen to induce tumor-specific T cell responses[27]. This allowed us to address whether the addition of IL2 to CTLA4+PD1 blockade resulted in a stronger expansion and activation of tumor-specific CD8$^+$ T cells. From the experiment shown in **Fig. 4A**, we performed longitudinal analysis of gp70 tetramer-specific CD8+ T cells in the peripheral blood of tumor-bearing mice pre- and post-treatment with either the dual combination therapy of anti-CTLA4+anti-PD1, triple combination therapy of anti-CTLA4+anti-PD1+IL2, IL2 alone, or control Ig (cIg) alone (**Fig. 4B and fig. S4**). We observed the greatest increase in gp70-specific T cells in mice treated with the triple combination therapy compared to either the dual checkpoint inhibitor combination therapy, IL2 alone, or cIg alone (**Fig. 4B**). Furthermore, the majority of gp70-specific T cells in the triple combination therapy treated group expressed CX3CR1 (**fig. S5A**) and KLRG1 (**fig. S5B**), suggesting a terminally differentiated T cell effector phenotype[28,29]. In addition, we observed an increase in non-gp70 tetramer reactive CD8$^+$ T cells expressing this effector phenotype in the triple combination therapy compared to the dual combination therapy-treated mice early after treatment, indicating a possible broadening of the tumor-specific T cell repertoire (**fig. S5, C and D**).

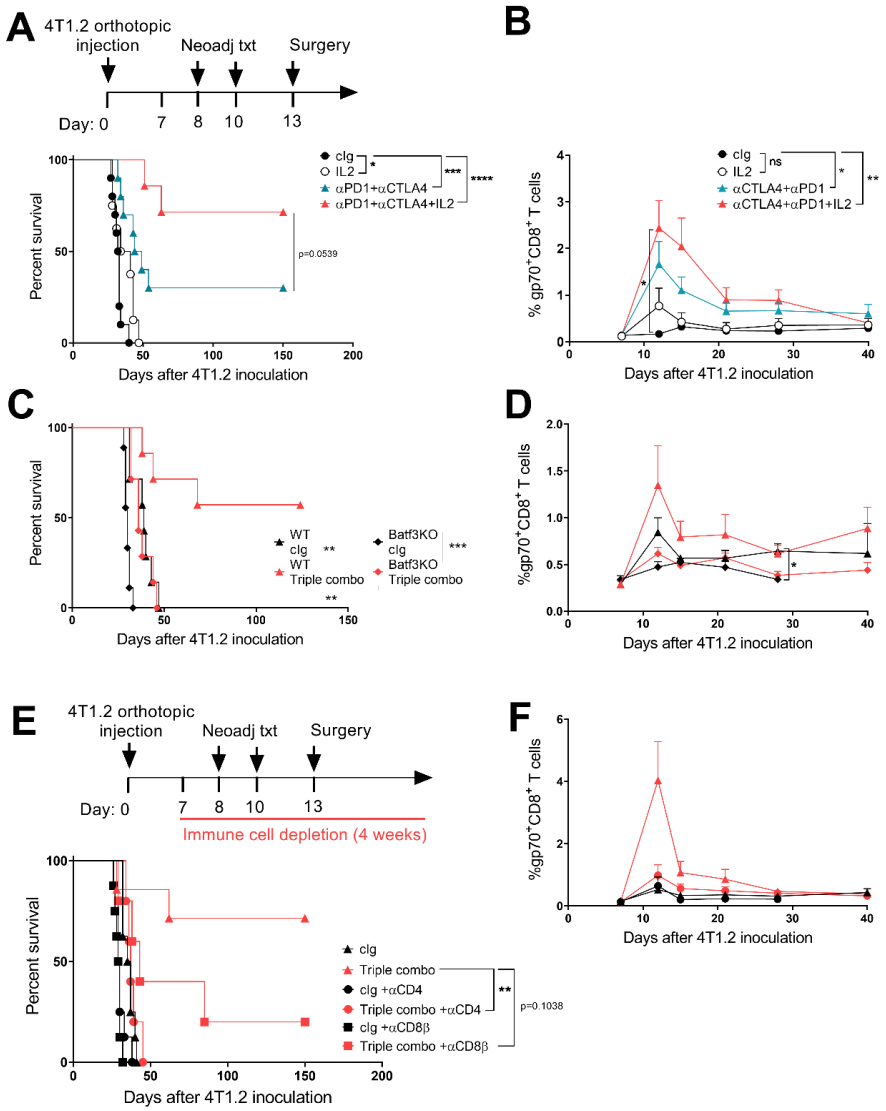

Figure 4. Addition of IL2 to neoadjuvant anti-CTLA4+anti-PD1 eradicates metastatic disease via improved expansion of tumor-specific CD8⁺ T cells. (A-B, E-F) Groups of BALB/c wild type (WT) or Batf3KO **(C-D)** mice were injected in the mammary fat pad with 4T1.2 tumor cells and treated i.p. on days 8 and 10 with the indicated combination of anti-CTLA4, anti-PD1, IL2 or clg followed by resection of the primary tumor on day 13 as indicated. **(E-F)** Additionally, some groups of mice were treated with clg, anti-CD4 or anti-CD8β on days 7, 8, 15, 22, and 29. **(A, C, E)** Kaplan-Meier curves for overall survival of each group are shown. **(B, D, F)** Proportion of gp70 tetramer⁺ CD8⁺ T cells in the blood of treated mice at the indicated time points (mean+SEM). **(A-F)** All experiments were double-blinded and performed once (n=5-10/group). Significant differences between the indicated groups were determined by **(A, C, E)** log-rank test or **(B, D, F)** mixed effects analysis with Tukey's multiple comparisons test. *P<0.05, **P<0.01, ***P<0.001, ****P<0.0001. Triple combo: anti-CTLA4+anti-PD1+IL2.

We next determined which innate and adaptive immune cells were important for the efficacy of neoadjuvant anti-CTLA4+anti-PD1+IL2 (**Fig. 4, C to F**). In a similar experimental setup as **Fig. 4A**, 4T1.2 tumor-bearing BATF3-deficient mice, which lack cross-presenting $CD103^+CD8\alpha^+$ DC were treated with neoadjuvant triple combination immunotherapy. These mice displayed a complete loss of long-term survivors compared to similar groups of treated tumor-bearing WT mice (**Fig. 4C**). This was supported by the lack of gp70-specific T cell expansion in the treated BATF3-deficient compared to WT mice (**Fig. 4D**). Furthermore, a requirement for both $CD4^+$ and $CD8^+$ T cells for the efficacy of neoadjuvant triple combination immunotherapy was also demonstrated (**Fig. 4, E and F**) by performing T cell specific depletions. $CD4^+$ T cell depletion in 4T1.2 tumor-bearing mice starting one day prior to commencement of neoadjuvant triple combination immunotherapy resulted in the complete loss of long term-survivors (0/5, 0%) compared to the cIg-treated triple neoadjuvant immunotherapy group (5/7, 71%) (**P<0.01) (**Fig. 4E**). This correlated with a lack of gp70-specific T cell expansion in the $CD4^+$ T cell-depleted group that was treated with the triple combination therapy (**Fig. 4F**). Similarly, $CD8^+$ T cell depletion prior to neoadjuvant anti-CTLA4+anti-PD1+IL2 treatment reduced the proportion of long-term survivors compared to the triple combination therapy treated group, although this abrogation of survival was not as striking as that seen with $CD4^+$ T cell depletion.

We next evaluated the importance of $CD4^+$ T cells in the priming of a natural $CD8^+$ T cell response prior to neoadjuvant immunotherapy or in the response against metastases after both surgery and treatment. We therefore set up a similar experiment as in **Fig. 4E**, where we depleted $CD4^+$ T cells at two different time points in neoadjuvant triple combination treated mice (**fig. S6**). In one group, $CD4^+$ T cell depletion began at day -1 prior to tumor inoculation (Triple combo+anti-CD4 d-1) and in the other group, depletion occurred one day after surgery at day 14 (Triple combo+anti-CD4 d14). There was no significant difference in survival between the group of mice in the triple combo+anti-CD4 d14 group and the non-CD4 depleted group ((5/11, 45% vs 7/12 (58%), respectively)) (**fig. S6A**). This suggests that the $CD4^+$ T cells helper or direct-killing functions may not be as critical to survival after primary tumor removal. In contrast, the triple combo+anti-CD4 d-1 group had significantly reduced survival compared to the non-CD4 depleted group (***P<0.001) (**fig. S6A**), similar to what we observed when depleting $CD4^+$ T cells at day 7 prior to neoadjuvant immunotherapy (**Fig. 4E**). In this experiment, we also measured longitudinally the proportion of gp70-specific CD8+ T cells in the blood, and we observed that only the mice from triple combo+anti-CD4 d-1 group failed to expand tumor-specific $CD8^+$ T cells in comparison to other triple combo treated groups (**fig. S6B**). Overall, these data and **Fig. 4E** suggest $CD4^+$ T cells are critical for priming of natural and treatment induced $CD8^+$ T cell immunity against 4T1.2 tumors and for helping in the expansion of gp70-tumor specific $CD8^+$ T cells early after neoadjuvant immunotherapy. However, they may not be as important following resection of the primary tumor.

To further investigate the mechanism by which IL2 improved the efficacy of neoadjuvant anti-CTLA4+anti-PD1, we set up an experiment similar to **Fig. 4**, where neoadjuvant triple

or double combination immunotherapy were compared and peripheral blood collected 2 days after the final treatment (**Fig. 5**). At the time point when the primary tumor is normally resected (day 13), we culled the mice, collected the primary tumor, spleen and draining lymph node and generated single cell suspensions for flow cytometry analyses (**Fig. 5**). As we previously observed in **Fig. 4B**, triple combination immunotherapy resulted in the greatest expansion of gp70-specific T cells in the peripheral blood compared to dual combination immunotherapy or IL2 alone (**P<0.01) (**fig. S7**). We observed the triple, compared to double, combination immunotherapy-treated group had an increased proportion of gp70$^+$ CD8$^+$ T cells, gp70neg CD8$^+$ T cells and CD4$^+$ T conventional (Tconv) cells that expressed intracellular IFN, TNF and IL2, which are typical proinflammatory cytokines (**Fig. 5, B to I and fig. S8**). A similar increase in proinflammatory cytokine polyfunctionality was also observed in CD4$^+$ FOXP3$^+$ cells, that are considered to be T regulatory (Tregs) cells (**Fig. 5, F to I**). Specifically, the triple combination immunotherapy compared to dual combination immunotherapy improved the quality of the different T cell subsets as measured by an increase in the expression of IFN-γ, IL2 and TNF (**fig. S9**). To determine whether the addition of IL2 to neoadjuvant anti-CTLA4+anti-PD1 treatment changed the phenotype of CD4+ Tconv and Tregs, we performed flow cytometry analysis for a number of surface markers of Tconv and Tregs from day 13 resected tumors (the time point we performed previous analyses for **Fig. 5**) (**fig. S10**). The markers we assessed included various co-stimulatory receptors (CD226, ICOS, CD137, OX40) or inhibitory receptors (CD39, CTLA4, NRP1, PD1, TIGIT). Overall, the changes observed in CD4+ Tconv and Treg phenotype were mainly due to neoadjuvant anti-CTLA4+anti-PD1 therapy, since the same trends were observed in both dual combination and triple combination treated groups (**fig. S10**). In conclusion, the addition of IL2 in the triple combination therapy works mainly by increasing the production of Th1 cytokines (**Fig. 5**), rather than changing co-stimulatory or inhibitory receptor expression on CD4$^+$ T cells.

To determine if the addition of IL2 to the dual combination immunotherapy improved proliferation, we also measured Ki67 staining on these T cell subsets. Overall, we observed an increase in the proliferation of all T cell subsets in the triple combination or dual combination immunotherapy groups compared to the cIg treated group in tumor, draining lymph node and spleen (**fig. S11**). However, there were no significant differences between triple combination or dual combination immunotherapy treated groups. We also observed no difference in the T cell subsets proportion in tumor infiltrating leukocytes following triple combination immunotherapy, dual combination immunotherapy or cIg treatment (**fig. S12A**). In the literature, it was reported that improved anti-tumor immunity in mouse models of cancer was associated with an increase in effector T cells to Treg ratio[30]. However, we observed no significant changes between the effector T cells to Treg ratio in immunotherapy treated and cIg treated groups (**fig. S12B**). Overall, our pre-clinical data demonstrated that the triple combination therapy of neoadjuvant anti-CTLA4+anti-PD1+IL2 compared to dual CTLA4+PD1 blockade cured a high proportion of mice with metastatic disease. This was due to improved expansion of tumor-specific CD8+ T cells, increased production of Th1 cytokines by total CD8+ and CD4+ T cells, and also by FOXP3+ CD4+ T cells.

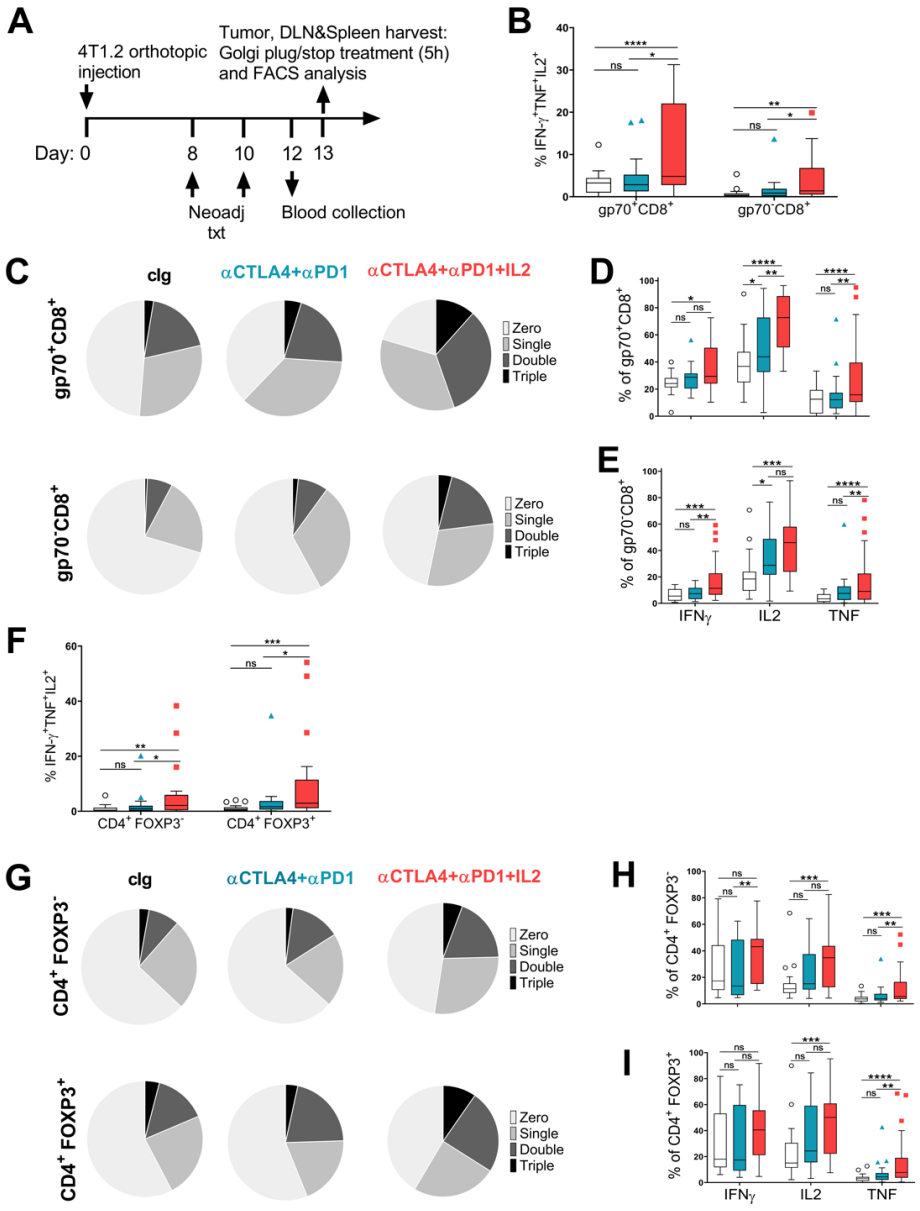

Figure 5. Addition of IL2 to neoadjuvant anti-CTLA4+anti-PD1 improves both CD8⁺ and CD4⁺ T cell cytokine polyfunctionality. (A-I) Groups of BALB/c wild type (WT) mice were injected in the mammary fat pad with 4T1.2 tumor cells and treated i.p on days 8 and 10 with the indicated combination of anti-CTLA4, anti-PD1, IL2 or cIg. On day 12, peripheral blood was collected from all groups of mice **(B)** and at day 13, tumors **(C-I)** were harvested and single cell suspensions generated for flow cytometry analysis. Gating on live CD45.2⁺ cells of leukocyte morphology, the proportion of the indicated **(B)** gp70 tetramer$^{+/-}$ CD8⁺ T cells or **(F)** CD4⁺ FOXP3⁻ (Tconv) or CD4⁺FOXP3⁺ (Treg) cells co-expressing intracellular IFNγ, TNF and IL2. Box plot with Tukey whiskers of **(C)** gp70 tetramer$^{+/-}$

$CD8^+$ T cells or **(G)** $CD4^+$ Tconv or Tregs expressing zero, one, two, or three cytokines (of IFNγ, TNF and IL2) or **(D, E, H, I)** the individual cytokines. Data pooled from 3 independent experiments that were performed and analyzed double-blinded (n=15-23/group). Statistical comparisons between groups were performed by 2-way ANOVA with Tukey's multiple comparisons test, *P<0.05, **P<0.01, ***P<0.001, ****P<0.0001.

Addition of IL2 to CTLA4+PD1 blockade induces immune responses in pretreatment biopsies from patients with melanoma resistant to neoadjuvant ipilimumab+nivolumab

To assess whether the addition of IL2 also induced immunological responses in CTLA4+PD1 blockade resistant tumors in the neoadjuvant clinical setting, we treated baseline biopsies from 16 patients with melanoma enrolled in the PRADO cohort of the OpACIN-neo trial (NCT02977052) with anti-CTLA4+anti-PD1+IL2 ex vivo. We were able to collect eight pre-treatment samples from patients who achieved a pathological response upon neoadjuvant ipilimumab+nivolumab (defined as pCR, near pCR or pPR; 'PRADO responder'), and eight pNR samples ('PRADO non-responder') (**table S4**). Due to the small size of the baseline biopsies (1x 12-14 g), assessment of responses was limited to the detection of soluble parameters in the unstimulated and anti-CTLA4+anti-PD1+IL2-treated conditions (**Fig. 6A**). As the smaller number of PDTFs per condition may induce more noise in the data, we aimed to identify the most relevant parameters for response by performing AUC analysis of each cytokine and chemokine secreted by the PDTFs from the resection cohort described in **Fig. 3**. This revealed that the separation of anti-CTLA4+anti-PD1 and anti-CTLA4+anti-PD1+IL2-responding and non-responding resected tumors was mostly driven by an increase in a subset of parameters, including IFN-γ, IL22 and CXCL10. This information was used to establish a response score based on the seven most discriminative parameters (**Fig. 6B and fig. S13**) to facilitate the classification of the biopsies as either responder or non-responder. Using this response score, we observed that anti-CTLA4+anti-PD1+IL2 induced an immunological response in 7/8 (87.5%) tumor biopsies from PRADO pathologic responders (**Fig. 6, C and D**), in line with the data obtained from tumor resections showing that tumors responding to dual checkpoint blockade also respond to the triple combination treatment (**Fig. 3, A and B)**. Within the PRADO pathologic non-responder group, treatment with the triple combination induced immunological responses in 5/8 (62.5%) of the tumor biopsies (**Fig. 6, C and D and fig. S14A**). For 12/16 biopsies, for which sufficient material was available, we also measured the release of six cytotoxic molecules (granulysin, granzyme A and B, perforin, sFas, sFasL) following anti-CTLA4+anti-PD1+IL2 treatment. The triple combination therapy increased the release of cytotoxic mediators in anti-CTLA4+anti-PD1 and anti-CTLA4+anti-PD1+IL2 responders, whereas no changes were observed in non-responding tumors (**Fig. 6E and fig. S14B**). Overall, these results suggest that the addition of IL2 to CTLA4+PD1 blockade may induce immune activation in tumors resistant to neoadjuvant anti-CTLA4+anti-PD1 that is comparable to those observed for responders to dual checkpoint blockade.

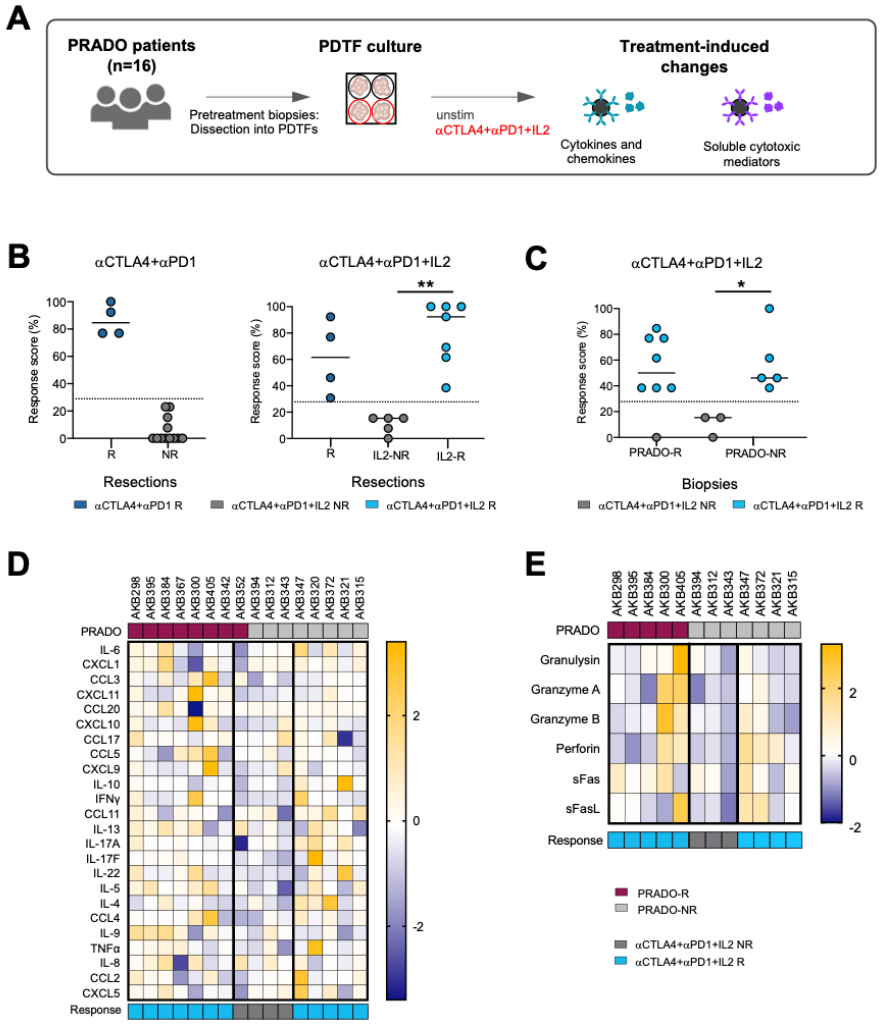

Figure 6. Addition of IL2 to CTLA4+PD1 blockade induces immunological responses in pretreatment biopsies of melanoma patients resistant to dual checkpoint blockade. (**A**) Schematic overview of the experimental outline using human tumor biopsies. **(B)** Response scores based on the parameters that best predict response for the anti-CTLA4+anti-PD1 and anti-CTLA4+anti-PD1+IL2 treatment groups derived from the 16 resected tumors from Fig. 3. **(C)** Response scores for each pretreatment melanoma tumor biopsy (n=16) collected from the PRADO trial, identifying three groups of tumors: αCTLA4+αPD1+IL2 R (within PRADO-R), αCTLA4+αPD1+IL2 NR and αCTLA4+αPD1+IL2 R (both within PRADO-NR). (**D)** Heatmap displaying the normalized delta values between the untreated and αCTLA4+αPD1+IL2 treated condition for each parameter (11 cytokines and 13 chemokines, n=16 pre-treatment tumor biopsies). The two groups were separated based on clinical response (pR vs pNR) to αCTLA4+αPD1. (**E)** Heatmap displaying the normalized delta values between the untreated and αCTLA4+αPD1+IL2 treated condition for six cytotoxic mediators (n=12 pre-treatment tumor biopsies from the PRADO cohort). Significant differences between groups were determined by or Mann-Whitney test (**B,** left) or Kruskal-Wallis test (**B**, right and **C**). *P<0.05, **P<0.01, ***P<0.001.

Discussion

Neoadjuvant checkpoint inhibition, and especially the combination of CTLA4+PD1 blockade, is currently the most promising therapeutic option for macroscopic stage III melanoma. Very high pathologic response rates of 71-80%, long-term RFS rates of 80% and overall survival of 90% have been observed in neoadjuvant checkpoint inhibitor treated patients with melanoma[6-8, 10]. This is in contrast to patients receiving surgery alone who are expected to have a RFS of 30% and 5-year overall survival in the range of 50%[31-33]. Even though the randomized registration trial comparing neoadjuvant ipilimumab+nivolumab versus adjuvant nivolumab (NADINA) has just started (end of 2021), two major questions remain: how to identify patients who will benefit from the current therapeutic options, and what alternative neoadjuvant combination therapy could be offered to patients with unfavorable tumor characteristics, who are unlikely to respond to neoadjuvant ipilimumab+nivolumab. We have recently shown that a high baseline IFN-γ signature and high tumor mutational burden were associated with 100% pathologic response and a subsequent extended RFS rate. In addition, having only one of the two favorable parameters was still associated with about 90% chance of response. In contrast, only 39% of patients lacking both factors responded[10]. Of note, the feasibility of applying such IFNγ-signature algorithms prospectively in trials to personalize neoadjuvant immunotherapy has recently been shown[34].

In search for rational treatment combinations for patients with melanoma who are unlikely to respond to neoadjuvant ipilimumab+nivolumab, we performed extended human RNA signature analyses. In addition to the previously described IFN-γ, T cell, and BATF3 signatures[4,12], we here found and confirmed in an independent cohort, a newly designed CD4/IL2 signature that correlated with outcome upon neoadjuvant ipilimumab+nivolumab. In a previous study, Raeber et al.,[16] utilized an IL2 signature derived from human T cells stimulated with IL2[35] to analyze The Cancer Genome Atlas (TCGA) data of a cohort of human skin cutaneous melanoma mostly derived from advanced cancers, comprising 20% primary cutaneous melanomas and 80% metastases[36]. They found that patients whose tumors displayed a high IL2 signature had prolonged survival[16]. In contrast, our CD4/IL2 signature derives from baseline pre-treatment tumor biopsies of patients with less advanced stage III melanoma. In addition to predicting patients who will respond to neoadjuvant ipilimumab+nivolumab, it will also be interesting to determine if our CD4/IL2 signature has prognostic or predictive value for patients with late-stage melanoma. Although the addition of IL2 has been shown to i) improve efficacy of checkpoint inhibition in large tumor burden mouse models, ii) decrease metastatic burden in 4T1 tumor-bearing mice, and iii) in late-stage disease of a patient in combination with adoptive TIL transfer[17, 18, 37], the efficacy of this combination has not been explored in any neoadjuvant setting. The strong predictive capability of the CD4/IL2 signature led us therefore to analyze the addition of IL2 to anti-CTLA4+anti-PD1 in a mouse tumor model of neoadjuvant immunotherapy and ex vivo in human tumor fragments. The triple combination immunotherapy compared to dual combination immunotherapy improved the activation and effector function of both $CD8^+$ and $CD4^+$ tumor-infiltrating lymphocytes as

measured by the upregulation of T cell activation markers and the co-expression of IFN-γ, TNF and IL2 in both human and murine settings. Although we previously demonstrated that the efficacy of neoadjuvant anti-PD1+anti-CD137 was dependent on presence of CD8+ T cells and partially dependent on $CD4^+$ T cells[3], herein, neoadjuvant anti-CTLA4+anti-PD1+IL2 was fully dependent on the presence of CD4+ T cells and partially dependent on CD8+ T cells. This may be due to the type of combination immunotherapy that was assessed in the current compared to our previous study. Furthermore, our data also suggested that these $CD4^+$ T cells were critical for the expansion of tumor-specific $CD8^+$ T cells since CD4 depletion prior to or early during neoadjuvant triple combination therapy completely abrogated their expansion in the blood, which was not the case when $CD4^+$ T cells were depleted post-surgery. Potentially these $CD4^+$ T cells may contribute to help $CD8^+$ T cell responses as previously reported[38], given the increased proportion of $CD4^+FOXP3^-$ helper T cells that produced IL2 following triple combination immunotherapy compared to dual combination immunotherapy. It is important to note that this effect may not be restricted to IL2, but may also be achieved by combining ICI with other cytokines that can overcome the lack of CD4 help and support $CD8^+$ T cell activation.

In addition to its role in stimulating conventional T cells, IL2 has been shown to promote the induction, survival and function of Tregs[24-26]. Importantly, in our study, the overall effects of adding IL2 to CTLA4+PD1 blockade were positive as observed by the increased proportion of effector $CD8^+$ and $CD4^+$ T cells with cytokine polyfunctionality (IFN-γ, TNF-α, IL2) and T cell proliferation in our mouse model. Similarly, in our ex vivo PDTF cultures, the addition of IL2 converted a proportion of anti-CTLA4+anti-PD1 immunological non-responders into responders as measured by the induction of a proinflammatory response including increased IFN-γ and TNF-α secretion. This response was induced despite the expansion of activated $CD4^+FOXP3^+$ T cells by the triple combination. Whether these $CD4^+FOXP3^+$ T cells represent true Tregs with suppressive function or CD4+ effector T cells that acquire FOXP3 expression during activation[39,40] will require further investigation. In mice, FOXP3 expression appears to be sufficient to define $CD4^+$ Tregs[41], but our pre-clinical data suggested that tumor-infiltrating Tregs from neoadjuvant anti-CTLA4+anti-PD1+IL2 treated mice also displayed a strong TH1 cytokine profile. Tregs producing IFN- γ despite retaining FOXP3 expression have previously been described to have a 'fragile' phenotype characterized by having reduced suppressive activity due to loss of Nrp1[42]. CD122-selective IL2 complexes were reported to reduce immunosuppression, promote Treg fragility, and sensitize tumor response to PD-L1 blockade[43]. However, it is unlikely this phenotype is the reason for the improved efficacy of neoadjuvant anti-CTLA4+anti-PD1+IL2 as these mice showed an increase in the proportion of Tregs expressing Nrp1 compared to those that received cIg or IL2. CTLA4 blockade in murine tumor models has recently been shown to promote functional destabilization of Tregs in poorly glycolytic tumor microenvironments (TMEs), which correlated with an improvement in CD8 effector function[44]. Similarly, PD1 blockade has been described to increase IFN-γ expression in Tregs[45]. Overall, both our animal and human data support the notion that, addition of IL2 to anti-CTLA4+anti-PD1 impacts anti-tumor immunity positively rather than negatively and can convert tumors from non-responsive to responsive to CTLA4+PD1 blockade.

To confirm our findings in a more relevant, thus neoadjuvant clinical setting, we assessed the effect of the triple combination immunotherapy in pretreatment biopsies of patients with stage III melanoma systemically treated with neoadjuvant ipilimumab+nivolumab. These experiments suggest that the triple combination of anti-CTLA4+anti-PD1+IL2 can induce immunological responses in about 50% of melanoma lesions from patients who are resistant to dual immune checkpoint blockade, thus providing a rationale to test this combination clinically.

Our study has some limitations. Although it would have been useful to demonstrate our pre-clinical findings in additional mouse cancer models, we utilized the 4T1.2 tumor model because it best mimics the clinical setting of surgery and therapy of residual metastatic disease as observed in patients with cancer, where it will result generally in death of mice if not treated. In contrast, carcinogen-induced and genetically modified mouse models as well as most transplant models of cancer do not offer this opportunity. Few truly metastasize, and metastasis is generally minimal relative to primary tumor size with late resection becoming impractical and unethical. Next, although we demonstrated pre-clinically the efficacy of neoadjuvant anti-CTLA4+anti-PD1+IL2 required the presence of Th1 cytokine producing $CD4^+$ T cells, it is unclear whether those $CD4^+$ T cells are tumor-reactive. More in-depth studies are required to understand the mechanisms by which CD4 T cells mediate anti-tumor efficacy in the neoadjuvant setting. Finally, in our study we combined dual checkpoint blockade with systemic IL2. Since systemic IL2 can induce potential toxicities, such as capillary leak syndrome caused by IL2s high affinity for CD25 (IL2Rα), which is expressed on the pulmonary vasculature[46], further investigation is necessary to avoid toxicity. One potential way to avoid toxicity would be to use intratumoral injection of IL2 or the use of targeted IL2 variants. Some examples include the CD25 mimobody which abolishes CD25 binding[47], variants that target IL2 to the tumor microenvironment[48], to effector CD8[49] or PD1 expressing T cells[50]. Taking into consideration a likely higher adverse event rate, one may preferentially test this triple combination immunotherapy in a personalized manner in patients with unfavorable tumor characteristics such as low TMB, low CD4/IL2 or IFN-γ signature. Moreover, given that TMB analyses are laborious, time consuming, and expensive, it will be important to compare their predictive value with our newly developed CD4/IL2 signature, as the latter may help to identify suitable patients in an easier manner. Potentially, the predictive value of this signature can also be evaluated in other cancer types where neoadjuvant ipilimumab+nivolumab is currently being tested[51-53].

Overall, our study shows how the combination of signature-driven analyses and functional assessment of patient tumor samples ex vivo, together with mechanistic experiments in in vivo mouse models can be used to identify potential treatment strategies for neoadjuvant combination checkpoint resistant melanoma. This study provides a rationale for testing the neoadjuvant combination of anti-CTLA4+anti-PD1+IL2 in patients with melanoma with unfavorable tumor characteristics.

Materials and Methods

Study design

This study was intended to examine whether additional IL2 immunotherapy can overcome resistance to neoadjuvant anti-CTLA4 and anti-PD1 in patients with melanoma. In pre-treatment biopsies from PRADO and OPACIN trials, we studied the gene signature associated with resistance to immune checkpoint blockade. Ex vivo stimulation of patient-derived tumor fragments were used to assess whether impaired response in resistant patients can be reversed by the addition of IL2. Pre-clinical studies in neoadjuvant-treated mice helped to decipher the mechanism by which addition of IL2 increased survival and induced a more potent anti-tumor immune response.

Patient characteristics and tumor sample processing

Resected tumor samples were collected from patients with cancer undergoing surgical treatment for melanoma, non-small cell lung cancer, ovarian cancer and renal cell carcinoma between April 2017 and October 2020 at the Netherlands Cancer Institute (NKI-AVL), The Netherlands (**table S3**). The study was approved by the institutional review board of the NKI-AVL (CFMPB484) and executed in compliance with the ethical regulations. All patients consented to the research usage of material not required for diagnostics either by opt-out procedure or via prior informed consent (after May 23, 2018). Pre-treatment tumor biopsies were collected from patients enrolled in the PRADO extension cohort of the OpACIN-neo trial (NCT02977052)[7] after obtaining written informed consent (**table S1 and S2**).

Resected tumor samples were collected in medium on ice (RPMI 1640 (Thermo Fisher) supplemented with 2.5% fetal bovine serum (FBS, Sigma), 1% Penicillin-Streptomycin (Roche)). Tumor samples were immediately dissected into fragments (patient-derived tumor fragments, PDTFs) of 1-2 mm3 on ice. PDTFs from different tumor areas were mixed and frozen in 1 mL freezing medium (FBS with 10% DMSO (Sigma)). Vials were cryopreserved in liquid nitrogen until usage. Tumor biopsies were processed in the same manner as resection samples. Pathological response upon neoadjuvant immunotherapy was assessed by a pathologist according to the International Neoadjuvant Melanoma Consortium scoring system[20].

RNA isolation and Nanostring data analysis

RNA was isolated from patients that had sufficient tumor material, based on the pathologist's scoring (at least 30% tumor cells of H&E stained cryostat frozen section), in the frozen tumor samples. RNA was simultaneously isolated from fresh-frozen pre-treatment tumor frozen sections (10 µm) with the AllPrep DNA/RNA/miRNA Universal isolation kit (Qiagen, 80224) using the QIAcube, according to the manufacturers' protocol. Gene expression analysis was conducted by using the Nanostring nCounter Analysis system and the PanCancer Immune Profiling panel which captures the read counts of 784 genes

(NanoString Technologies, Seattle, WA, USA). Raw counts were normalized to internal expression of 38 reference genes: *ABCF1, AGK, ALAS1, AMMECR1L, CC2D1B, CNOT10, CNOT4, COG7, DDX50, DHX16, EDC3, EIF2B4, ERCC3, FCF1, G6PD, GPATCH3, GUSB, HDAC3, HPRT1, MRPS5, MTMR14, NOL7, NUBP1, POLR2A, PPIA, PRPF38A, SAP130, SDHA, SF3A3, TBP, TLK2, TMUB2, TRIM39, TUBB, USP39, ZC3H14, ZKSCAN5, ZNF143*. A background count was estimated using the average count of the 8 negative control probes in every reaction plus 2 SDs. Next, the CD4/IL2, CD8 (Danaher) and BATF3 subset genes signature scores were calculated from the average z-score of all the genes within each signature separately per patient. The optimal cutoff to determine patients with CD8/BATF3 high or low signature score was computed by the sROC curves for each signature independently on PRADO and OpACIN neo cohorts together (n=143). Pearson's correlation method was employed to compute the correlation coefficients.

Patient-derived tumor fragment (PDTF) cultures

PDTF cultures were performed as described previously (23). In brief, cryo-preserved PDTFs were thawed, extensively washed with wash medium (DMEM supplemented with 10% FBS and 1% Penicillin-Streptomycin) and embedded in an artificial extracellular matrix (sodium bicarbonate (Sigma, 1.1%), collagen I (Corning, 1 mg/mL), matrigel (Matrix High Concentration, Phenol Red-Free, BD Biosciences, 4 mg/mL), tumor medium (DMEM supplemented with 1mM sodium pyruvate (Sigma), 1× MEM non-essential AA (Sigma), 2 mM L-glutamine (Thermo Fisher), 10% FBS and 1% Penicillin-Streptomycin)) in a flat-bottom 96-well plate. PDTF cultures were topped up with tumor medium supplemented with either anti-PD1 (nivolumab, Bristol-Myers Squibb) at 10 µg/mL, anti-CTLA4 (ipilimumab, Bristol-Myers Squibb) at 10 µg/mL and 3000 pg/mL (~60 IU/mL) recombinant human IL2 (rhIL2, Proleukin, PeproTech) where indicated. rhIL2 concentration was chosen based on IL2 plasma concentrations after subcutaneous (s.c.) rhIL2 treatment[54,55]. After 48 hours of culture at 37°C, supernatants were collected and immediately frozen at -80°C for subsequent cytokine and chemokine analysis. PDTFs were pooled and subjected to flow analysis for assessment of immune cell activation (see below).

Tissue processing and flow cytometric analysis of human samples

PDTFs were collected in 2 mL digestion mix (RPMI 1640 with 1% Penicillin-Streptomycin, 12.6 µg/mL Pulmozyme (Roche) and 1 mg/mL Collagenase type IV (Sigma)) on ice. PDTFs were digested at 37°C while rotating for 45-60 min, washed with PBS and filtered. The remaining single cell suspensions were transferred to a 96-well plate for the staining procedure. Before antibody staining, cells were incubated with human FcR Blocking Reagent (eBioscience) for 20 min on ice. Cells were stained with live/dead IR Dye (Thermo Fisher) or Zombie UV (Biolegend) for 20 min on ice, washed, and incubated with the surface antibody mix in FACS buffer (PBS, 0.5% bovine serum albumin (Sigma), 0.1% NaN3 (Invitrogen)) for 20 min on ice. All antibodies used are listed in table S5. After washing, cells were fixed and permeabilized using the Fix/Perm solution (eBioscience) for 30 min at room temperature. Cells were subsequently washed twice with 1× Permeabilization buffer (eBioscience) and

incubated with intracellular antibody mix in Permeabilization buffer for 40 min at room temperature. Cells were washed twice and resuspended in FACS buffer for data acquisition. For the quantification of immune cell subsets, cells were gated on live (IRDye negative) and single cells. Cells were identified as non-immune cells (CD45 negative) and immune cells ($CD45^+$). Within CD3- immune cells, B cells were gated as $CD19^+$, NK cells as CD16+, and myeloid cells as CD11b+. T cells were gated as $CD3^+$. These were divided into conventional $CD4^+$ T cells ($FOXP3^-$), regulatory T cells ($FOXP3^+$), $CD8^+$ T cells and NKT-like cells ($CD16^+$). For assessment of T cell activation, cells were gated on live (IRDye negative) and single cells. $CD45^+CD3^+$ T cells were subdivided into CD8+, $CD4^+FOXP3^-$ and $CD4^+FOXP3^+$ T cell subsets. Within each subset, CD137 and OX40 expression were quantified. Flow cytometric analyses were performed using an LSR II SORP and BD LSRFortessa (BD Bioscience). Flowjo analysis software (v10.6.2) was used for data analysis.

Analysis of cytokines and chemokines and cytotoxic mediators

Supernatants collected from PDTF cultures were thawed on ice and pooled for each experimental condition. Presence of indicated cytokines and chemokines was detected using the LEGENDplex™ Human Th Cytokine and Human Proinflammatory Chemokine panels (both Biolegend). Cytotoxic mediators were measured using the LEGENDplex™ Human CD8/NK panel (Biolegend). All assays were performed according to the manufacturer's protocol.

Mice

BALB/c wild-type (WT) and BALB/c Batf3-deficient mice were bred and maintained at the QIMR Berghofer Medical Research Institute. Female mice 8 weeks and older were used in all experiments and performed in accordance to QIMR Berghofer Medical Research Institute animal experimental ethics committee guidelines.

Cell line

BALB/c-derived 4T1.2 mammary carcinoma were maintained in RPMI supplemented with 10% FCS, penicillin/streptomycin, and additional L-glutamine (Gibco, Waltham, USA) as previously described[3]. All cell lines were routinely tested as negative for mycoplasma. Cell line authentication was not routinely performed.

Experimental tumor model

Following 4T1.2 orthotopic tumor inoculation into the mammary fat pad, and prior to extensive primary tumor growth, mice develop a substantial burden of metastases in the lungs, liver, bones, and brain, among other organs[3]. Female BALB/c WT mice were injected in the 4th or 5th mammary fat pad with 5×104 4T1.2 cells. Prior to the surgical resection of the primary tumor and tumor draining lymph node as previously described[3], mice were treated intraperitoneally (i.p.) with 200 µg rat control IgG2a (1-1) or a combination of 100 µg anti-PD1 (RMP1-14), 100 µg anti-CTLA4 (UC10-4F10-11), 50,000 IU rhIL2 (Proleukin S) (see table S6 for reference). For immune cell depletion experiments, mice were additionally

treated with cIg (1-1), anti-CD4 (GK1.5) or anti-CD8β (53-5.8) as indicated in the figure legends. Mice were monitored for symptoms of illness with changes to posture, activity, breathing, and fur texture, and euthanized when clinical symptoms reached the cumulative limit outlined by animal ethics. Mice were randomly assigned to treatment groups. All experiments were performed and analyzed double-blinded as indicated in the figure legends.

Flow cytometry- mouse

Tumors, blood, spleen, and draining lymph nodes (DLN) were harvested from mice and processed for flow cytometry analysis as previously described[27]. For surface staining, tumor-infiltrating lymphocyte or immune cell suspensions were stained with antibodies and respective isotype antibodies in the presence of anti-CD16/32 (2.4G2) to block FcR. The list of flow cytometry antibodies used is described in table S6. To stain for Ki67 and FoxP3, samples were fixed and permeabilized with a FOXP3 Fixation/Permeabilization Kit (eBioscience). To measure intracellular cytokine staining, single-cell suspensions were incubated for 5 hours in complete RPMI with monensin and brefeldin A (eBioscience). Samples were then surface stained before being fixed/permeabilized (BD CytoFix/ CytoPerm Kit) and stained with anti-IFNγ, anti-TNF and anti-IL2. All data were collected on a LSRFortessa (Becton Dickinson) flow cytometer and analyzed with FlowJo v10 software (Tree Star, Inc.). Gating strategy shown in **Fig. S4 and S8**.

Statistical analysis

Mouse

Statistical analysis was performed using GraphPad Prism software V.9. Differences between indicated mouse groups were determined by 2-way ANOVA (or mixed effects analysis when appropriate) test with Tukey's correction as indicated. Differences between survival curves were determined using a log-rank test. P-values were considered significant with $P<0.05$ indicated with (*), $P<0.01$ with (**), $P<0.001$ with (***) and $P< 0.0001$ with (****). For all studies, biological replicates and number of independently performed experiments are indicated in the figure legends. Mouse exclusion criteria were predetermined as follows: 4T1.2 bearing mice were excluded if mice were culled solely due to ethical endpoints not related to 4T1.2 breast cancer metastases. In flow cytometric analyses, samples containing <20 gp70-tetramer+ CD8+ T cell events were excluded from downstream analyses (**Fig. 5, B and D and fig. S5, A and B and S9A and S11, A to C**).

Human

Statistical analysis was performed using GraphPad Prism software V.9. Differences between indicated treatment groups were determined by Mann-Whitney test or Kruskal-Wallis test as indicated. P-values were considered significant with $P<0.05$ indicated with (*), $P<0.01$ with (**), $P<0.001$ with (***) and $P< 0.0001$ with (****). Sample size was described for each test separately and based on the availability of patient samples for

the analysis. Identification of PDTF responder and non-responder groups was performed using the built-in unsupervised clustering function in R (v4.0.2). Response patterns in each group were validated in an independent replicate PDTF culture. The IL2 response score was developed by first calculating receiver operating characteristic (ROC) curves based on the delta values for each parameter measured in the pooled dataset of responders and non-responders to the anti-CTLA4+anti-PD1 combination and the anti-CTLA4+anti-PD1+IL2 triple combination. Seven parameters that were strongly discriminative between responders and non-responders were selected based on the area under the ROC curve (AUROC). For each parameter, a cut-off value was identified aiming for high specificity and sensitivity. This cut-off was used to score each parameter in each sample depending whether the delta value was above or below the cut-off.

The response score was calculated as follows:
IL2 response score = (∑(sum of all parameters))/(maximal score)×100

Data and materials availability

All data associated with this study are present in the paper or supplementary materials.

References

1. J. M. Versluis, G. V. Long, C. U. Blank, Learning from clinical trials of neoadjuvant checkpoint blockade. Nat. Med. 26, 475-484 (2020).
2. C. U. Blank, J. B. Haanen, A. Ribas, T. N. Schumacher, CANCER IMMUNOLOGY. The"cancer immunogram". Science 352, 658-660 (2016).
3. J. Liu, S. J. Blake, M. C. Yong, H. Harjunpaa, S. F. Ngiow, K. Takeda, A. Young, J. S.O'Donnell, S. Allen, M. J. Smyth, M. W. Teng, Improved efficacy of neoadjuvant compared to adjuvant immunotherapy to eradicate metastatic disease. Cancer Discov. 6, 1382-1399(2016).
4. C. U. Blank, E. A. Rozeman, L. F. Fanchi, K. Sikorska, B. van de Wiel, P. Kvistborg, O.Krijgsman, M. van den Braber, D. Philips, A. Broeks, J. V. van Thienen, H. A. Mallo, S. Adriaansz, S. Ter Meulen, L. M. Pronk, L. G. Grijpink-Ongering, A. Bruining, R. M. Gittelman, S. Warren, H. van Tinteren, D. S. Peeper, J. Haanen, A. C. J. van Akkooi, T. N. Schumacher, Neoadjuvant versus adjuvant ipilimumab plus nivolumab in macroscopic stage III melanoma.Nat. Med. 24, 1655-1661 (2018).
5. A. C. Huang, R. J. Orlowski, X. Xu, R. Mick, S. M. George, P. K. Yan, S. Manne, A. A. Kraya, B. Wubbenhorst, L. Dorfman, K. D'Andrea, B. M. Wenz, S. Liu, L. Chilukuri, A. Kozlov, M. Carberry, L. Giles, M. W. Kier, F. Quagliarello, S. McGettigan, K. Kreider, L. Annamalai, Q. Zhao, R. Mogg, W. Xu, W. M. Blumenschein, J. H. Yearley, G. P. Linette, R. K. Amaravadi, L. M. Schuchter, R. S. Herati, B. Bengsch, K. L. Nathanson, M. D. Farwell, G. C. Karakousis, E. J. Wherry, T. C. Mitchell, A single dose of neoadjuvant PD-1 blockade predicts clinical outcomes in resectable melanoma. Nat. Med. 25, 454-461 (2019).
6. R. N. Amaria, S. M. Reddy, H. A. Tawbi, M. A. Davies, M. I. Ross, I. C. Glitza, J. N. Cormier, C. Lewis, W. J. Hwu, E. Hanna, A. Diab, M. K. Wong, R. Royal, N. Gross, R. Weber, S. Y. Lai, R. Ehlers, J. Blando, D. R. Milton, S. Woodman, R. Kageyama, D. K. Wells, P. Hwu, S. P. Patel, A. Lucci, A. Hessel, J. E. Lee, J. Gershenwald, L. Simpson, E. M. Burton, L. Posada, L. Haydu, L. Wang, S. Zhang, A. J. Lazar, C. W. Hudgens, V. Gopalakrishnan, A. Reuben, M. C. Andrews, C. N. Spencer, V. Prieto, P. Sharma, J. Allison, M. T. Tetzlaff, J. A. Wargo, Neoadjuvant immune checkpoint blockade in high-risk resectable melanoma. Nat. Med. 24, 1649-1654 (2018).
7. E. A. Rozeman, A. M. Menzies, A. C. J. van Akkooi, C. Adhikari, C. Bierman, B. A. van de Wiel, R. A. Scolyer, O. Krijgsman, K. Sikorska, H. Eriksson, A. Broeks, J. V. van Thienen, A. D. Guminski, A. T. Acosta, S. Ter Meulen, A. M. Koenen, L. J. W. Bosch, K. Shannon, L. M. Pronk, M. Gonzalez, S. Ch'ng, L. G. Grijpink-Ongering, J. Stretch, S. Heijmink, H. van Tinteren, J. Haanen, O. E. Nieweg, W. M. C. Klop, C. L. Zuur, R. P. M. Saw, W. J. van Houdt, D. S. Peeper, A. J. Spillane, J. Hansson, T. N. Schumacher, G. V. Long, C. U. Blank, Identification of the optimal combination dosing schedule of neoadjuvant ipilimumab plus nivolumab in macroscopic stage III melanoma (OpACIN-neo): a multicentre, phase 2, randomised, controlled trial. Lancet Oncol. 20, 948-960 (2019).
8. C. U. Blank, I. L. M. Reijers, T. Pennington, J. M. Versluis, R. P. Saw, E. A. Rozeman, E. Kapiteijn, A. A. M. V. D. Veldt, K. Suijkerbuijk, G. Hospers, W. M. C. Klop, K. Sikorska, J. A. V. D. Hage, D. J. Grunhagen, A. Spillane, R. V. Rawson, B. A. V. D. Wiel, A. M. Menzies, A. C. J. V. Akkooi, G. V. Long, First safety and efficacy results of PRADO: A phase II study of personalized response-driven surgery and adjuvant therapy after neoadjuvant ipilimumab (IPI) and nivolumab (NIVO) in resectable stage III melanoma. J. Clin. Oncol. 38, 10002-10002 (2020).
9. A. M. Menzies, R. N. Amaria, E. A. Rozeman, A. C. Huang, M. T. Tetzlaff, B. A. van de Wiel, S. Lo, A. A. Tarhini, E. M. Burton, T. E. Pennington, R. P. M. Saw, X. Xu, G. C. Karakousis, P. A. Ascierto, A. J. Spillane, A. C. J. van Akkooi, M. A. Davies, T. C. Mitchell, H. A. Tawbi, R. A. Scolyer, J. A. Wargo, C. U. Blank, G. V. Long, Pathological response and survival with neoadjuvant therapy in melanoma: a pooled analysis from the International Neoadjuvant Melanoma Consortium (INMC). Nat. Med. 27, 301-309 (2021).

10. E. A. Rozeman, E. P. Hoefsmit, I. L. M. Reijers, R. P. M. Saw, J. M. Versluis, O. Krijgsman, P. Dimitriadis, K. Sikorska, B. A. van de Wiel, H. Eriksson, M. Gonzalez, A. Torres Acosta, L. G. Grijpink-Ongering, K. Shannon, J. Haanen, J. Stretch, S. Ch'ng, O. E. Nieweg, H. A. Mallo, S. Adriaansz, R. M. Kerkhoven, S. Cornelissen, A. Broeks, W. M. C. Klop, C. L. Zuur, W. J. van Houdt, D. S. Peeper, A. J. Spillane, A. C. J. van Akkooi, R. A. Scolyer, T. N. M. Schumacher, A. M. Menzies, G. V. Long, C. U. Blank, Survival and biomarker analyses from the OpACIN-neo and OpACIN neoadjuvant immunotherapy trials in stage III melanoma. Nat. Med. 27, 256-263 (2021).
11. E. A. Rozeman, L. Fanchi, A. C. J. van Akkooi, P. Kvistborg, J. V. Thienen, B. Stegenga, B. Lamon, J. B. Haanen, T. N. M. Schumacher, C. U. Blank, paper presented at the 42nd ESMO Congress, Madrid, Spain, 8 to 12 September 2017.
12. J. Liu, E. A. Rozeman, J. S. O'Donnell, S. Allen, L. Fanchi, M. J. Smyth, C. U. Blank, M. W. L. Teng, Batf3(+) DCs and type I IFN are critical for the efficacy of neoadjuvant cancer immunotherapy. Oncoimmunology 8, e1546068 (2019).
13. J. Borst, T. Ahrends, N. Babala, C. J. M. Melief, W. Kastenmuller, CD4(+) T cell help in cancer immunology and immunotherapy. Nat. Rev. Immunol. 18, 635-647 (2018).
14. W. Liao, J. X. Lin, W. J. Leonard, Interleukin-2 at the crossroads of effector responses, tolerance, and immunotherapy. Immunity 38, 13-25 (2013).
15. P. Loetscher, M. Seitz, M. Baggiolini, B. Moser, Interleukin-2 regulates CC chemokine receptor expression and chemotactic responsiveness in T lymphocytes. J. Exp. Med. 184, 569-577 (1996).
16. M. E. Raeber, R. A. Rosalia, D. Schmid, U. Karakus, O. Boyman, Interleukin-2 signals converge in a lymphoid-dendritic cell pathway that promotes anticancer immunity. Sci. Transl. Med. 12, eaba5464 (2020).
17. K. D. Moynihan, C. F. Opel, G. L. Szeto, A. Tzeng, E. F. Zhu, J. M. Engreitz, R. T. Williams, K. Rakhra, M. H. Zhang, A. M. Rothschilds, S. Kumari, R. L. Kelly, B. H. Kwan, W. Abraham, K. Hu, N. K. Mehta, M. J. Kauke, H. Suh, J. R. Cochran, D. A. Lauffenburger, K. D. Wittrup, D. J. Irvine, Eradication of large established tumors in mice by combination immunotherapy that engages innate and adaptive immune responses. Nat. Med. 22, 1402-1410 (2016).
18. N. Zacharakis, H. Chinnasamy, M. Black, H. Xu, Y. C. Lu, Z. Zheng, A. Pasetto, M. Langhan, T. Shelton, T. Prickett, J. Gartner, L. Jia, K. Trebska-McGowan, R. P. Somerville, P. F. Robbins, S. A. Rosenberg, S. L. Goff, S. A. Feldman, Immune recognition of somatic mutations leading to complete durable regression in metastatic breast cancer. Nat. Med. 24, 724-730 (2018).
19. L. S. Cheung, J. Fu, P. Kumar, A. Kumar, M. E. Urbanowski, E. A. Ihms, S. Parveen, C. K. Bullen, G. J. Patrick, R. Harrison, J. R. Murphy, D. M. Pardoll, W. R. Bishai, Second-generation IL-2 receptor-targeted diphtheria fusion toxin exhibits antitumor activity and synergy with anti-PD-1 in melanoma. Proc. Natl. Acad. Sci. U.S.A. 116, 3100-3105 (2019).
20. M. T. Tetzlaff, J. L. Messina, J. E. Stein, X. Xu, R. N. Amaria, C. U. Blank, B. A. van de Wiel, P. M. Ferguson, R. V. Rawson, M. I. Ross, A. J. Spillane, J. E. Gershenwald, R. P. M. Saw, A. C. J. van Akkooi, W. J. van Houdt, T. C. Mitchell, A. M. Menzies, G. V. Long, J. A. Wargo, M. A. Davies, V. G. Prieto, J. M. Taube, R. A. Scolyer, Pathological assessment of resection specimens after neoadjuvant therapy for metastatic melanoma. Ann. Oncol. 29, 1861-1868 (2018).
21. P. Danaher, S. Warren, L. Dennis, L. D'Amico, A. White, M. L. Disis, M. A. Geller, K. Odunsi, J. Beechem, S. P. Fling, Gene expression markers of Tumor Infiltrating Leukocytes. J. Immunother. Cancer 5, 18 (2017).
22. S. Spranger, D. Dai, B. Horton, T. F. Gajewski, Tumor-Residing Batf3 Dendritic Cells Are Required for Effector T Cell Trafficking and Adoptive T Cell Therapy. Cancer Cell 31, 711-723.e714 (2017).
23. P. Voabil, M. de Bruijn, L. M. Roelofsen, S. H. Hendriks, S. Brokamp, M. van den Braber, A. Broeks, J. Sanders, P. Herzig, A. Zippelius, C. U. Blank, K. J. Hartemink, K. Monkhorst, J. Haanen, T. N. Schumacher, D. S. Thommen, An ex vivo tumor fragment platform to dissect response to PD-1 blockade in cancer. Nat. Med. 27, 1250-1261 (2021).
24. A. K. Abbas, E. Trotta, R. S. D, A. Marson, J. A. Bluestone, Revisiting IL-2: Biology and therapeutic prospects. Sci. Immunol. 3, eaat1482 (2018).

25. J. P. Dutcher, D. J. Schwartzentruber, H. L. Kaufman, S. S. Agarwala, A. A. Tarhini, J. N. Lowder, M. B. Atkins, High dose interleukin-2 (Aldesleukin) - expert consensus on best management practices-2014. J. Immunother. Cancer 2, 26 (2014).
26. M. Ahmadzadeh, S. A. Rosenberg, IL-2 administration increases CD4+ CD25(hi) Foxp3+ regulatory T cells in cancer patients. Blood 107, 2409-2414 (2006).
27. J. Liu, J. S. O'Donnell, J. Yan, J. Madore, S. Allen, M. J. Smyth, M. W. L. Teng, Timing of neoadjuvant immunotherapy in relation to surgery is crucial for outcome. Oncoimmunology 8, e1581530 (2019).
28. N. S. Joshi, W. Cui, A. Chandele, H. K. Lee, D. R. Urso, J. Hagman, L. Gapin, S. M. Kaech, Inflammation directs memory precursor and short-lived effector CD8(+) T cell fates via the graded expression of T-bet transcription factor. Immunity 27, 281-295 (2007).
29. C. Gerlach, E. A. Moseman, S. M. Loughhead, D. Alvarez, A. J. Zwijnenburg, L. Waanders, R. Garg, J. C. de la Torre, U. H. von Andrian, The Chemokine Receptor CX3CR1 Defines Three Antigen-Experienced CD8 T Cell Subsets with Distinct Roles in Immune Surveillance and Homeostasis. Immunity 45, 1270-1284 (2016).
30. M. J. Selby, J. J. Engelhardt, M. Quigley, K. A. Henning, T. Chen, M. Srinivasan, A. J. Korman, Anti-CTLA-4 antibodies of IgG2a isotype enhance antitumor activity through reduction of intratumoral regulatory T cells. Cancer Immunol. Res. 1, 32-42 (2013).
31. J. E. Gershenwald, R. A. Scolyer, K. R. Hess, V. K. Sondak, G. V. Long, M. I. Ross, A. J. Lazar, M. B. Faries, J. M. Kirkwood, G. A. McArthur, L. E. Haydu, A. M. M. Eggermont, K. T. Flaherty, C. M. Balch, J. F. Thompson, Melanoma staging: Evidence-based changes in the American Joint Committee on Cancer eighth edition cancer staging manual. CA: Cancer J. Clin. 67, 472-492 (2017).
32. A. C. van Akkooi, M. G. Bouwhuis, A. N. van Geel, R. Hoedemaker, C. Verhoef, D. J. Grunhagen, P. I. Schmitz, A. M. Eggermont, J. H. de Wilt, Morbidity and prognosis after therapeutic lymph node dissections for malignant melanoma. Eur. J. Surg. Oncol. 33, 102-108 (2007).
33. A. P. van der Ploeg, A. C. van Akkooi, P. I. Schmitz, A. N. van Geel, J. H. de Wilt, A. M. Eggermont, C. Verhoef, Therapeutic surgical management of palpable melanoma groin metastases: superficial or combined superficial and deep groin lymph node dissection. Ann. Surg. Oncol. 18, 3300-3308 (2011).
34. I. L. M. Reijers, P. Dimitriadis, E. A. Rozeman, J. M. Versluis, A. Broeks, L. J. W. Bosch, J. Bouwman, S. Cornelissen, O. Krijgsman, M. Gonzalez, D. S. Rao, L. G. Grijpink-Ongering, M. van Dijk, A. Spillane, R. A. Scolyer, B. A. Van de Wiel, A. M. Menzies, A. C. J. Van Akkooi, G. V. Long, C. U. Blank, paper presented at the ASCO Virtual Scientific Program, Chicago, IL, 29 to 31 May 2020.
35. P. E. Kovanen, L. Young, A. Al-Shami, V. Rovella, C. A. Pise-Masison, M. F. Radonovich, J. Powell, J. Fu, J. N. Brady, P. J. Munson, W. J. Leonard, Global analysis of IL-2 target genes: identification of chromosomal clusters of expressed genes. Int. Immunol. 17, 1009-1021 (2005).
36. R. Akbani, Kadir C. Akdemir, B. A. Aksoy, M. Albert, A. Ally, Samirkumar B. Amin, H. Arachchi, A. Arora, J. T. Auman, B. Ayala, J. Baboud, M. Balasundaram, S. Balu, N. Barnabas, J. Bartlett, P. Bartlett, Boris C. Bastian, Stephen B. Baylin, M. Behera, D. Belyaev, C. Benz, B. Bernard, R. Beroukhim, N. Bir, Aaron D. Black, T. Bodenheimer, L. Boice, Genevieve M. Boland, R. Bono, Moiz S. Bootwalla, M. Bosenberg, J. Bowen, R. Bowlby, Christopher A. Bristow, L. Brockway-Lunardi, D. Brooks, J. Brzezinski, W. Bshara, E. Buda, William R. Burns, Yaron S. N. Butterfield, M. Button, T. Calderone, Giancarlo A. Cappellini, C. Carter, Scott L. Carter, L. Cherney, Andrew D. Cherniack, A. Chevalier, L. Chin, J. Cho, Raymond J. Cho, Y.-L. Choi, A. Chu, S. Chudamani, K. Cibulskis, G. Ciriello, A. Clarke, S. Coons, L. Cope, D. Crain, E. Curley, L. Danilova, S. D'Atri, T. Davidsen, Michael A. Davies, Keith A. Delman, John A. Demchok, Qixia A. Deng, Yonathan L. Deribe, N. Dhalla, R. Dhir, D. DiCara, M. Dinikin, M. Dubina, J. S. Ebrom, S. Egea, G. Eley, J. Engel, Jennifer M. Eschbacher, Konstantin V. Fedosenko, I. Felau, T. Fennell, Martin L. Ferguson, S. Fisher, Keith T. Flaherty, S. Frazer, J. Frick, V. Fulidou, Stacey B. Gabriel, J. Gao, J. Gardner, Levi A. Garraway, Julie M. Gastier-Foster, C. Gaudioso, N. Gehlenborg, G. Genovese, M. Gerken, Jeffrey E. Gershenwald, G. Getz, C. Gomez-Fernandez, T. Gribbin, J. Grimsby, B. Gross, R. Guin, T. Gutschner, A. Hadjipanayis,

R. Halaban, B. Hanf, D. Haussler, Lauren E. Haydu, D. N. Hayes, Nicholas K. Hayward, David I. Heiman, L. Herbert, James G. Herman, P. Hersey, Katherine A. Hoadley, E. Hodis, Robert A. Holt, Dave S. Hoon, S. Hoppough, Alan P. Hoyle, Franklin W. Huang, M. Huang, S. Huang, Carolyn M. Hutter, M. Ibbs, L. Iype, A. Jacobsen, V. Jakrot, A. Janning, William R. Jeck, Stuart R. Jefferys, Mark A. Jensen, Corbin D. Jones, Steven J. M. Jones, Z. Ju, H. Kakavand, H. Kang, Richard F. Kefford, Fadlo R. Khuri, J. Kim, John M. Kirkwood, J. Klode, A. Korkut, K. Korski, M. Krauthammer, R. Kucherlapati, Lawrence N. Kwong, W. Kycler, M. Ladanyi, Phillip H. Lai, Peter W. Laird, E. Lander, Michael S. Lawrence, Alexander J. Lazar, R. Łaźniak, D. Lee, Jeffrey E. Lee, J. Lee, K. Lee, S. Lee, W. Lee, E. Leporowska, Kristen M. Leraas, Haiyan I. Li, Tara M. Lichtenberg, L. Lichtenstein, P. Lin, S. Ling, J. Liu, O. Liu, W. Liu, Georgina V. Long, Y. Lu, S. Ma, Y. Ma, A. Mackiewicz, Harshad S. Mahadeshwar, J. Malke, D. Mallery, Georgy M. Manikhas, Graham J. Mann, Marco A. Marra, B. Matejka, M. Mayo, S. Mehrabi, S. Meng, M. Meyerson, Piotr A. Mieczkowski, John P. Miller, Martin L. Miller, Gordon B. Mills, F. Moiseenko, Richard A. Moore, S. Morris, C. Morrison, D. Morton, S. Moschos, Lisle E. Mose, Florian L. Muller, Andrew J. Mungall, D. Murawa, P. Murawa, Bradley A. Murray, L. Nezi, S. Ng, D. Nicholson, Michael S. Noble, A. Osunkoya, Taofeek K. Owonikoko, Bradley A. Ozenberger, E. Pagani, Oxana V. Paklina, A. Pantazi, M. Parfenov, J. Parfitt, Peter J. Park, W.-Y. Park, Joel S. Parker, F. Passarelli, R. Penny, Charles M. Perou, Todd D. Pihl, O. Potapova, Victor G. Prieto, A. Protopopov, Michael J. Quinn, A. Radenbaugh, K. Rai, Suresh S. Ramalingam, Ayush T. Raman, Nilsa C. Ramirez, R. Ramirez, U. Rao, W. K. Rathmell, X. Ren, Sheila M. Reynolds, J. Roach, A. G. Robertson, Merrick I. Ross, J. Roszik, G. Russo, G. Saksena, C. Saller, Y. Samuels, C. Sander, C. Sander, G. Sandusky, N. Santoso, M. Saul, Robyn P. Saw, D. Schadendorf, Jacqueline E. Schein, N. Schultz, Steven E. Schumacher, C. Schwallier, Richard A. Scolyer, J. Seidman, Pedamallu C. Sekhar, Harmanjatinder S. Sekhon, Y. Senbabaoglu, S. Seth, Kerwin F. Shannon, S. Sharpe, Norman E. Sharpless, Kenna R. M. Shaw, C. Shelton, T. Shelton, R. Shen, M. Sheth, Y. Shi, Carolyn J. Shiau, I. Shmulevich, Gabriel L. Sica, Janae V. Simons, R. Sinha, P. Sipahimalani, Heidi J. Sofia, Matthew G. Soloway, X. Song, C. Sougnez, Andrew J. Spillane, A. Spychała, Jonathan R. Stretch, J. Stuart, Wiktoria M. Suchorska, A. Sucker, S. O. Sumer, Y. Sun, M. Synott, B. Tabak, Teresa R. Tabler, A. Tam, D. Tan, J. Tang, R. Tarnuzzer, K. Tarvin, H. Tatka, Barry S. Taylor, M. Teresiak, N. Thiessen, John F. Thompson, L. Thorne, V. Thorsson, Jeffrey M. Trent, Timothy J. Triche, Kenneth Y. Tsai, P. Tsou, David J. Van Den Berg, Eliezer M. Van Allen, U. Veluvolu, Roeland G. Verhaak, D. Voet, O. Voronina, V. Walter, Jessica S. Walton, Y. Wan, Y. Wang, Z. Wang, S. Waring, Ian R. Watson, N. Weinhold, John N. Weinstein, Daniel J. Weisenberger, P. White, Matthew D. Wilkerson, James S. Wilmott, L. Wise, M. Wiznerowicz, Scott E. Woodman, C.-J. Wu, C.-C. Wu, J. Wu, Y. Wu, R. Xi, Andrew W. Xu, D. Yang, L. Yang, L. Yang, Travis I. Zack, Jean C. Zenklusen, H. Zhang, J. Zhang, W. Zhang, X. Zhao, J. Zhu, K. Zhu, L. Zimmer, E. Zmuda, L. Zou, Genomic Classification of Cutaneous Melanoma. Cell 161, 1681-1696 (2015).

37. D. Sahin, N. Arenas-Ramirez, M. Rath, U. Karakus, M. Humbelin, M. van Gogh, L. Borsig, O. Boyman, An IL-2-grafted antibody immunotherapy with potent efficacy against metastatic cancer. Nat. Commun. 11, 6440 (2020).

38. E. B. Wilson, A. M. Livingstone, Cutting edge: CD4+ T cell-derived IL-2 is essential for help-dependent primary CD8+ T cell responses. J. Immunol. 181, 7445-7448 (2008).

39. M. A. Gavin, T. R. Torgerson, E. Houston, P. DeRoos, W. Y. Ho, A. Stray-Pedersen, E. L. Ocheltree, P. D. Greenberg, H. D. Ochs, A. Y. Rudensky, Single-cell analysis of normal and FOXP3-mutant human T cells: FOXP3 expression without regulatory T cell development. Proc. Natl. Acad. Sci. U.S.A. 103, 6659-6664 (2006).

40. M. E. Morgan, J. H. van Bilsen, A. M. Bakker, B. Heemskerk, M. W. Schilham, F. C. Hartgers, B. G. Elferink, L. van der Zanden, R. R. de Vries, T. W. Huizinga, T. H. Ottenhoff, R. E. Toes, Expression of FOXP3 mRNA is not confined to CD4+CD25+ T regulatory cells in humans. Hum. Immunol. 66, 13-20 (2005).

41. J. M. Kim, J. P. Rasmussen, A. Y. Rudensky, Regulatory T cells prevent catastrophic autoimmunity throughout the lifespan of mice. Nat. Immunol. 8, 191-197 (2007).

42. A. E. Overacre-Delgoffe, M. Chikina, R. E. Dadey, H. Yano, E. A. Brunazzi, G. Shayan, W. Horne, J. M. Moskovitz, J. K. Kolls, C. Sander, Y. Shuai, D. P. Normolle, J. M. Kirkwood, R. L. Ferris, G. M. Delgoffe, T. C. Bruno, C. J. Workman, D. A. A. Vignali, Interferon-γ Drives T(reg) Fragility to Promote Anti-tumor Immunity. Cell 169, 1130-1141.e1111 (2017).
43. J. M. Drerup, Y. Deng, S. L. Pandeswara, A. S. Padron, R. M. Reyes, X. Zhang, J. Mendez, A. Liu, C. A. Clark, W. Chen, J. R. Conejo-Garcia, V. Hurez, H. Gupta, T. J. Curiel, CD122-Selective IL2 Complexes Reduce Immunosuppression, Promote Treg Fragility, and Sensitize Tumor Response to PD-L1 Blockade. Cancer Res. 80, 5063-5075 (2020).
44. R. Zappasodi, I. Serganova, I. J. Cohen, M. Maeda, M. Shindo, Y. Senbabaoglu, M. J. Watson, A. Leftin, R. Maniyar, S. Verma, M. Lubin, M. Ko, M. M. Mane, H. Zhong, C. Liu, A. Ghosh, M. Abu-Akeel, E. Ackerstaff, J. A. Koutcher, P. C. Ho, G. M. Delgoffe, R. Blasberg, J. D. Wolchok, T. Merghoub, CTLA-4 blockade drives loss of T(reg) stability in glycolysis-low tumours. Nature 591, 652-658 (2021).
45. S. A. Lim, J. Wei, T. M. Nguyen, H. Shi, W. Su, G. Palacios, Y. Dhungana, N. M. Chapman, L. Long, J. Saravia, P. Vogel, H. Chi, Lipid signalling enforces functional specialization of T(reg) cells in tumours. Nature 591, 306-311 (2021).
46. C. Krieg, S. Letourneau, G. Pantaleo, O. Boyman, Improved IL-2 immunotherapy by selective stimulation of IL-2 receptors on lymphocytes and endothelial cells. Proc. Natl. Acad. Sci. U.S.A. 107, 11906-11911 (2010).
47. N. Arenas-Ramirez, C. Zou, S. Popp, D. Zingg, B. Brannetti, E. Wirth, T. Calzascia, J. Kovarik, L. Sommer, G. Zenke, J. Woytschak, C. H. Regnier, A. Katopodis, O. Boyman, Improved cancer immunotherapy by a CD25-mimobody conferring selectivity to human interleukin-2. Sci. Transl. Med. 8, 367ra166 (2016).
48. I. Waldhauer, V. Gonzalez-Nicolini, A. Freimoser-Grundschober, T. K. Nayak, L. Fahrni, R. J. Hosse, D. Gerrits, E. J. W. Geven, J. Sam, S. Lang, E. Bommer, V. Steinhart, E. Husar, S. Colombetti, E. Van Puijenbroek, M. Neubauer, J. M. Cline, P. K. Garg, G. Dugan, F. Cavallo, G. Acuna, J. Charo, V. Teichgraber, S. Evers, O. C. Boerman, M. Bacac, E. Moessner, P. Umana, C. Klein, Simlukafusp alfa (FAP-IL2v) immunocytokine is a versatile combination partner for cancer immunotherapy. MAbs 13, 1913791 (2021).
49. H. Sultan, K. Moynihan, Y. Song, S. Ameh, T. Schumacher, Y. A. Yeung, I. Djuretic, R. Schreiber, 578 CD8-targeted IL-2 drives potent anti-tumor efficacy and promotes action of tumor specific vaccines. J. Immunother. Cancer 9, A607-A607 (2021).
50. Z. Ren, A. Zhang, Z. Sun, Y. Liang, J. Ye, J. Qiao, B. Li, Y. X. Fu, Selective delivery of low-affinity IL-2 to PD-1+ T cells rejuvenates antitumor immunity with reduced toxicity. J. Clin. Invest. 132, e153604 (2022).
51. M. Chalabi, L. F. Fanchi, K. K. Dijkstra, J. G. Van den Berg, A. G. Aalbers, K. Sikorska, M. Lopez-Yurda, C. Grootscholten, G. L. Beets, P. Snaebjornsson, M. Maas, M. Mertz, V. Veninga, G. Bounova, A. Broeks, R. G. Beets-Tan, T. R. de Wijkerslooth, A. U. van Lent, H. A. Marsman, E. Nuijten, N. F. Kok, M. Kuiper, W. H. Verbeek, M. Kok, M. E. Van Leerdam, T. N. Schumacher, E. E. Voest, J. B. Haanen, Neoadjuvant immunotherapy leads to pathological responses in MMR-proficient and MMR-deficient early-stage colon cancers. Nat. Med. 26, 566-576 (2020).
52. N. van Dijk, A. Gil-Jimenez, K. Silina, K. Hendricksen, L. A. Smit, J. M. de Feijter, M. L. van Montfoort, C. van Rooijen, D. Peters, A. Broeks, H. G. van der Poel, A. Bruining, Y. Lubeck, K. Sikorska, T. N. Boellaard, P. Kvistborg, D. J. Vis, E. Hooijberg, T. N. Schumacher, M. van den Broek, L. F. A. Wessels, C. U. Blank, B. W. van Rhijn, M. S. van der Heijden, Preoperative ipilimumab plus nivolumab in locoregionally advanced urothelial cancer: the NABUCCO trial. Nat. Med. 26, 1839-1844 (2020).

53. T. Cascone, W. N. William, Jr., A. Weissferdt, C. H. Leung, H. Y. Lin, A. Pataer, M. C. B. Godoy, B. W. Carter, L. Federico, A. Reuben, M. A. W. Khan, H. Dejima, A. Francisco-Cruz, E. R. Parra, L. M. Solis, J. Fujimoto, H. T. Tran, N. Kalhor, F. V. Fossella, F. E. Mott, A. S. Tsao, G. Blumenschein, Jr., X. Le, J. Zhang, F. Skoulidis, J. M. Kurie, M. Altan, C. Lu, B. S. Glisson, L. A. Byers, Y. Y. Elamin, R. J. Mehran, D. C. Rice, G. L. Walsh, W. L. Hofstetter, J. A. Roth, M. B. Antonoff, H. Kadara, C. Haymaker, C. Bernatchez, N. J. Ajami, R. R. Jenq, P. Sharma, J. P. Allison, A. Futreal, J. A. Wargo, Wistuba, II, S. G. Swisher, J. J. Lee, D. L. Gibbons, A. A. Vaporciyan, J. V. Heymach, B. Sepesi, Neoadjuvant nivolumab or nivolumab plus ipilimumab in operable non-small cell lung cancer: the phase 2 randomized NEOSTAR trial. Nat. Med. 27, 504-514 (2021).

54. G. I. Kirchner, A. Franzke, J. Buer, W. Beil, M. Probst-Kepper, F. Wittke, K. Overmann, S. Lassmann, R. Hoffmann, H. Kirchner, A. Ganser, J. Atzpodien, Pharmacokinetics of recombinant human interleukin-2 in advanced renal cell carcinoma patients following subcutaneous application. Br. J. Clin. Pharmacol. 46, 5-10 (1998).55. O. Eton, M. G. Rosenblum, S. S. Legha, W. Zhang, M. Jo East, A. Bedikian, N. Papadopoulos, A. Buzaid, R. S. Benjamin, Phase I trial of subcutaneous recombinant human interleukin-2 in patients with metastatic melanoma. Cancer 95, 127-134 (2002).

56. C. Thiele, G. Hirschfeld, cutpointr: Improved Estimation and Validation of Optimal Cutpoints in R. J. Stat. Softw. 98, 1-27 (2021).

Supplementary figures

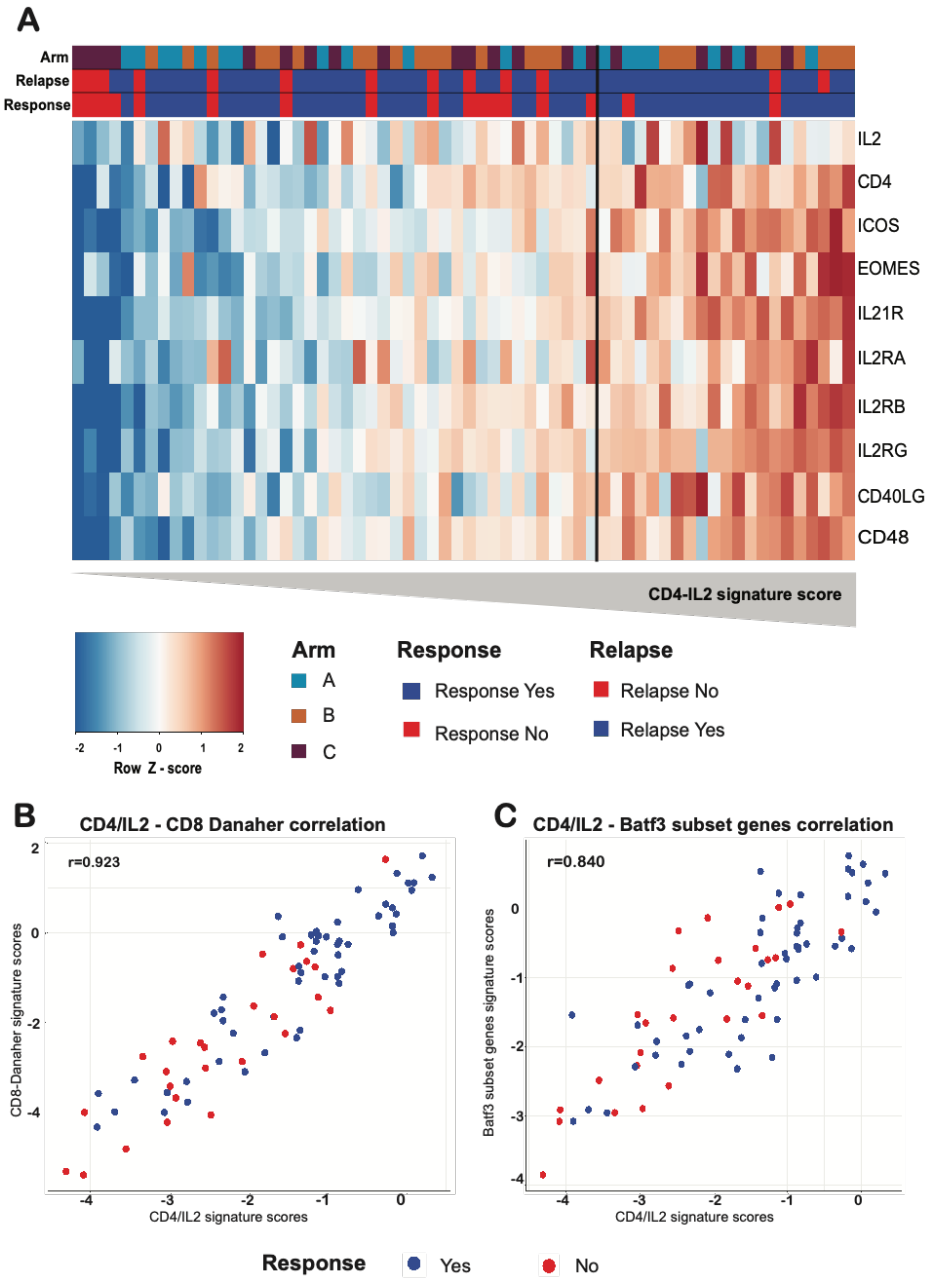

Figure S1. A CD4/IL2 gene signature is associated with response to neoadjuvant ipilimumab + nivolumab – Validation cohort. **(A)** Nanostring data of pre-treatment lymph node tumor biopsies of patients treated with neoadjuvant ipilimumab+nivolumab in the OpACIN-neo study (n=64). The

heatmap of the CD4/IL2 gene signature is ordered according to the average expression of the CD4/IL2 gene signature per patient. Each column displays one patient (blue: pathologic response /no relapse, red: no pathologic response/relapse, blue: treatment arm A (2x IPI 3 mg/kg + NIVO 1 mg/kg q3wk), orange: treatment arm B (2× IPI 1 mg/kg + NIVO 3 mg/kg q3wk), purple: treatment arm C (2× IPI 3 mg/kg q3wk followed by 2 × NIVO 3 mg/kg q2wk)). The rows in the heatmap represents the z-score of the gene expressions of each of the 10 genes that compose it. Next, the signature score is calculated from the average expression of all the 10 genes per patient. Positive values (red) imply higher gene expression and negative values (blue) indicate lower gene expression. The threshold to define a high CD4/IL2 score is indicated by the black vertical line. **(B** and **C)** Correlation between **(B)** CD4/IL2 and CD8 (Danaher) score or **(C)** CD4/IL2 and BATF3 subset genes score in the PRADO cohort as described in Fig. 1. Values displayed as the average z-score of all the genes within the CD4/IL2, CD8 (Danaher) and BATF3 subset genes signature. Patients with pathologic response are depicted with blue dots and patients without pathologic response with red dots. The correlation coefficient was calculated using the Pearson's correlation method.

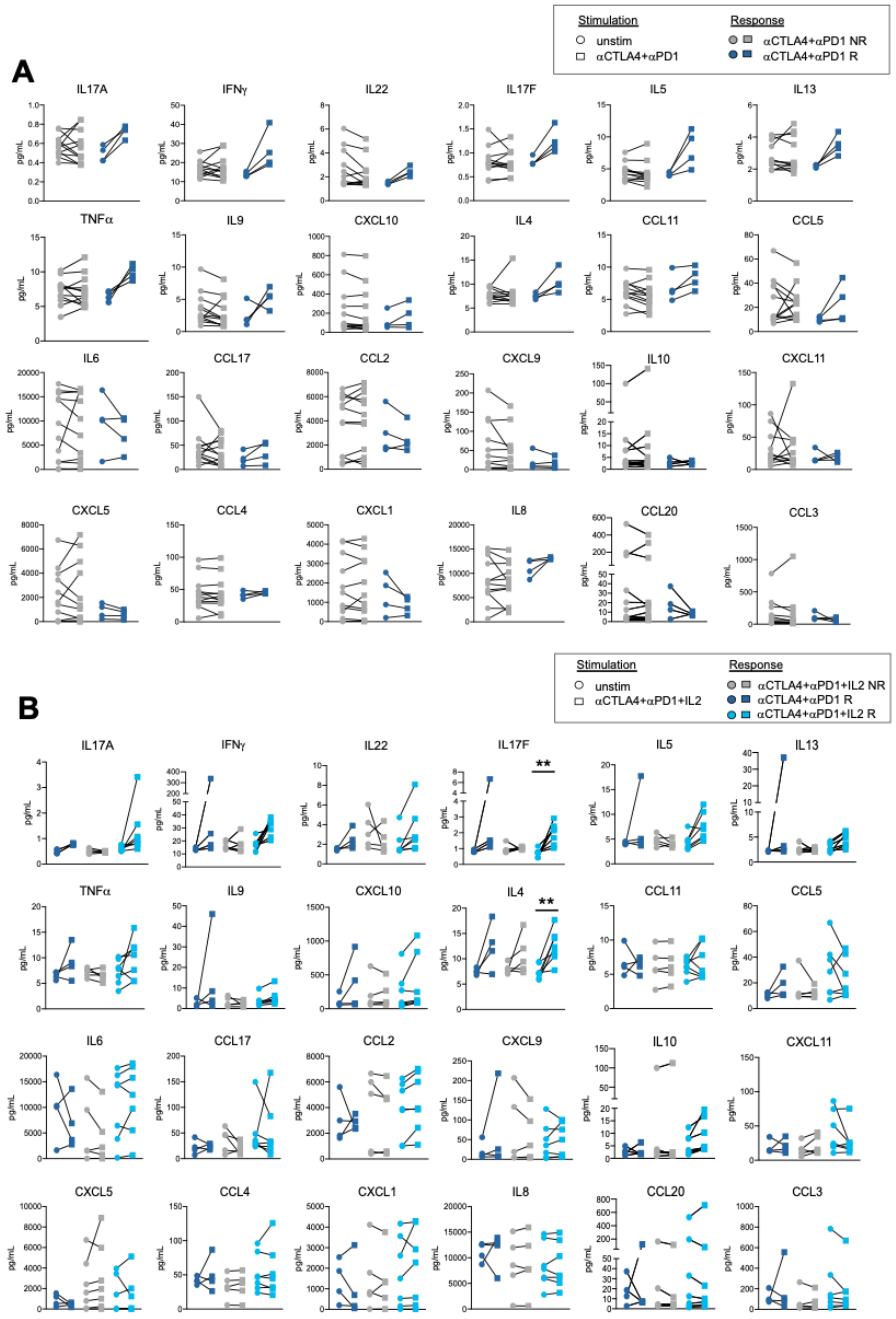

Figure S2. Soluble markers secreted by PDTFs of the tumor resection cohort upon ex vivo treatment. Related to Fig. 3. Cytokines and chemokines assessed in **(A)** untreated and anti(α)-CTLA4+αPD1 and in **(B)** untreated and αCTLA4+αPD1+IL2 treated PDTFs. Parameters are displayed separately for responders and non-responders to the dual and triple combination treatments, respectively. Significant differences between groups were determined by Kruskal-Wallis test. $^{**}P<0.01$

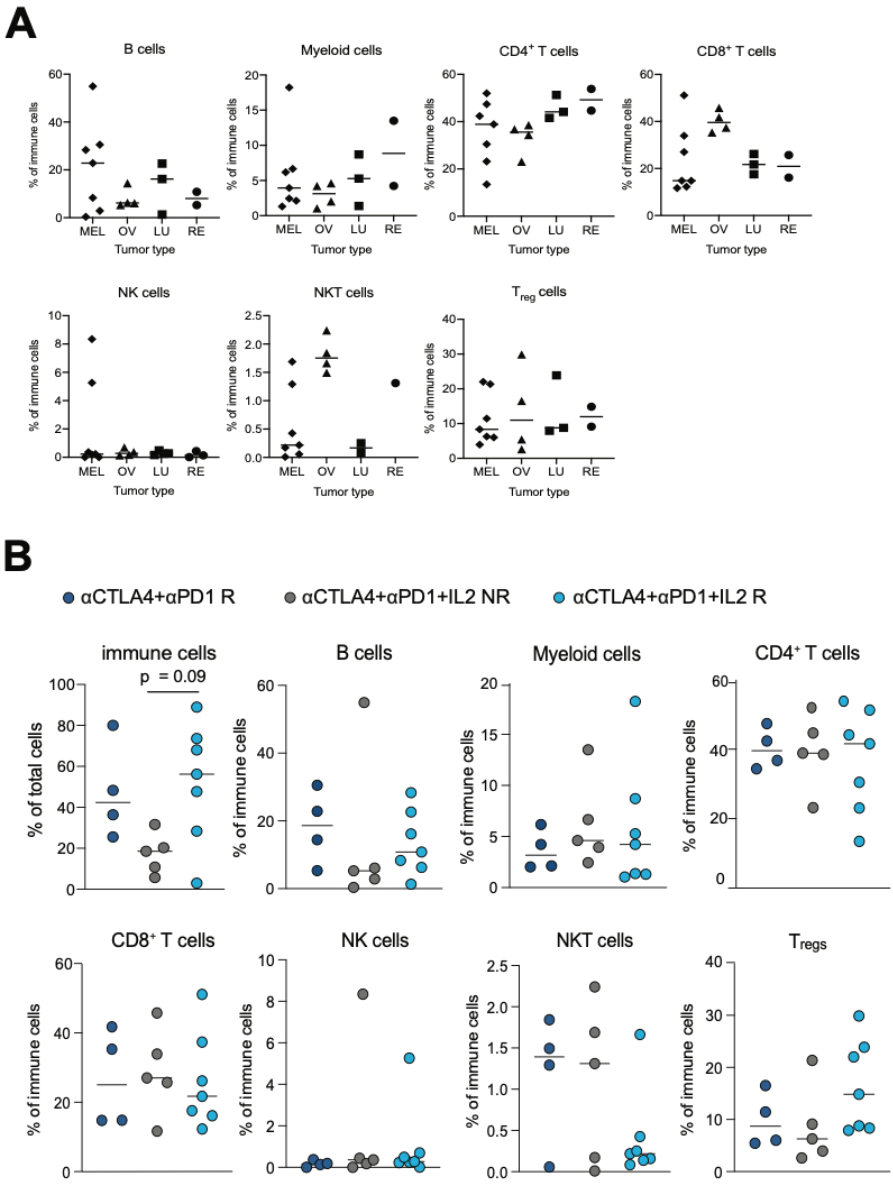

Figure S3. Baseline immune cell composition of the PDTFs from the tumor resection cohort. Related to Fig. 3. **(A)** Quantification of various immune cell subsets assessed by flow cytometry within total live cells per tumor type: melanoma (MEL), ovarian cancer (OV), non-small cell lung cancer (LU) and renal cell carcinoma (RE) and **(B)** for the response groups αCTLA4+αPD1 R, αCTLA4+αPD1+IL2 NR and αCTLA4+αPD1+IL2 R. The line indicates the mean. Significant differences between groups were determined by Kruskal-Wallis test.

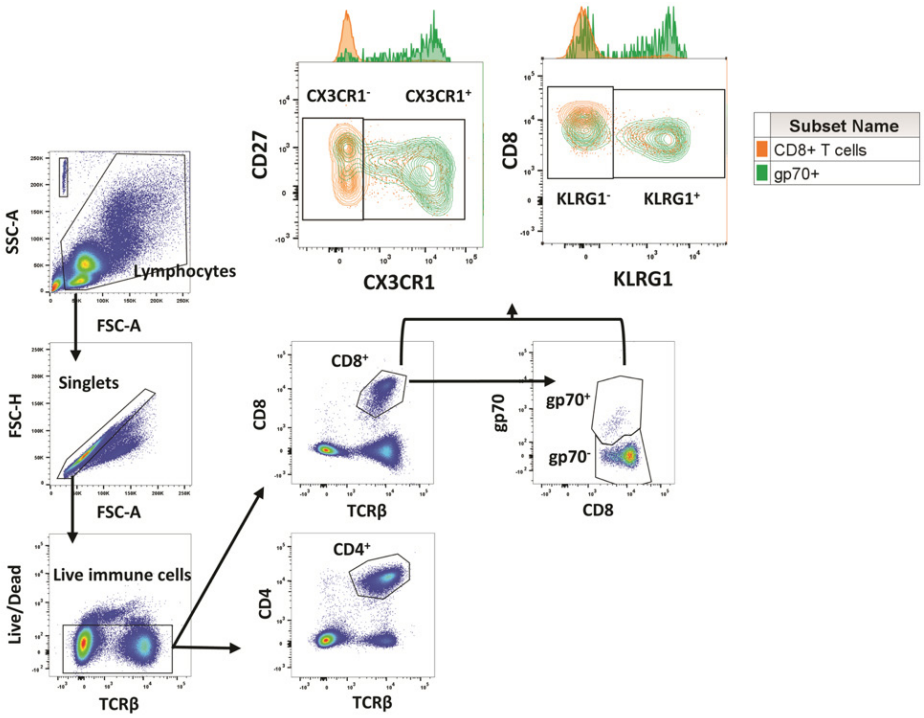

Figure S4. Gating strategy for gp70⁺CD8⁺ T cells in blood. From the same experiment as described in Fig. 4B. Gating strategy for total CD8⁺ T cells and gp70⁺ subsets. These representative dot plots are from a blood sample taken at day 12 on a mouse treated with anti-CTLA+anti-PD1+IL2. Gating strategy for CX3CR1⁺ and KLRG1⁺ subpopulations are represented (see fig. S5).

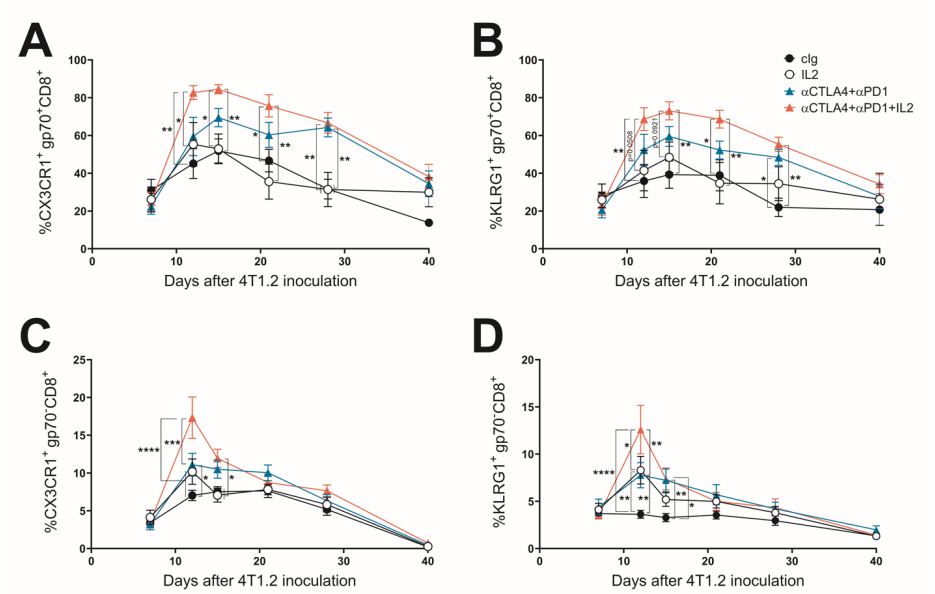

Figure S5. Addition of IL2 to neoadjuvant anti-CTLA4+anti-PD1 improves expansion of CX3CR1$^+$ or KLRG1$^+$ T cells in mice. From the same experiment as described in Fig. 4B. **(A** to **D)** Proportion of CX3CR1$^+$ and KLRG1$^+$ expressing cells within **(A** and **B)** gp70$^+$ CD8$^+$ T cells and **(C** and **D)** gp70$^-$ CD8$^+$ T cells in the peripheral blood at the indicated time points. Experiment was blinded and performed once (*n*=7-10/group; mean±SEM). Significant differences between double or triple combination groups compared to other treatment groups at each time point were determined by mixed effects analysis with Tukey's multiple comparisons test. **P*<0.05, ***P*<0.01, ****P*<0.001, ****P<0.0001.

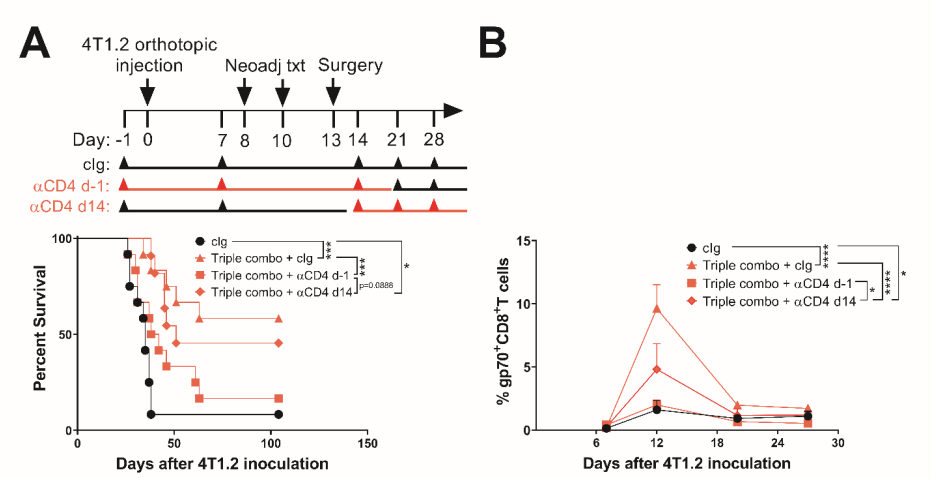

Figure S6. CD4 T cells are required for the efficacy of neoadjuvant anti-CTLA4+anti-PD1+IL2. **(A** and **B)** Groups of BALB/c wild type (WT) mice were injected in the mammary fat pad with 4T1.2 tumor cells and treated i.p. on days 8 and 10 with anti-CTLA4+anti-PD1+IL2 (Triple combo) or cIg followed by resection of the primary tumor on day 13. The triple combo treated mice were randomized into 3 groups receiving either anti-CD4 on days -1, 7, 14 and cIg on days 21, 28 or cIg on days -1, 7 and anti-CD4 on days 14, 21, 28 or cIg on days -1, 7, 14, 21, 28 post 4T1.2 tumor inoculation as indicated in the schematic. **(A)** Kaplan-Meier curves for overall survival of each group are shown. **(B)** Proportion of gp70 tetramer$^+$ CD8$^+$ T cells in the blood of treated mice at the indicated time points (mean±SEM). All experiments were double-blinded and performed once (n=11-12/group). Significant differences between the indicated groups were determined by **(A)** log-rank test or **(B)** mixed effects analysis with Tukey's multiple comparisons test. *P<0.05, *** P <0.001, **** P <0.0001.

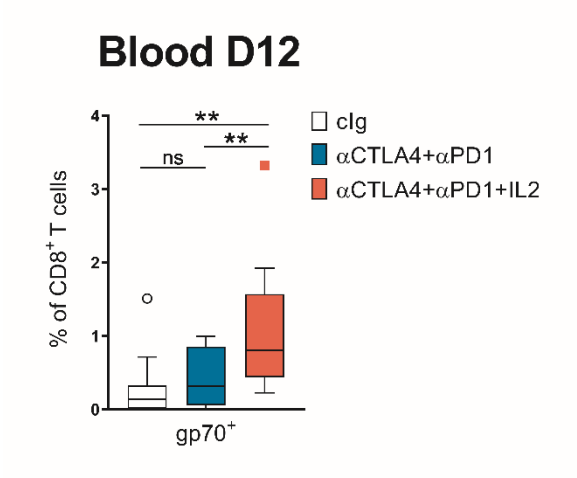

Figure S7. Addition of IL2 to neoadjuvant anti-CTLA4+anti-PD1 expands tumor-specific CD8⁺ T cells in the blood of mice. From the same experiment as Fig. 5, the proportion of gp70⁺ CD8⁺ T cells in the blood of the indicated treated groups collected at day 12 post-tumor inoculation. Data pooled from 2 independent experiments performed and analyzed double-blinded (*n*=15/group). Statistical comparisons between groups were performed by 2-way ANOVA with Tukey's multiple comparisons test, ** P <0.01.

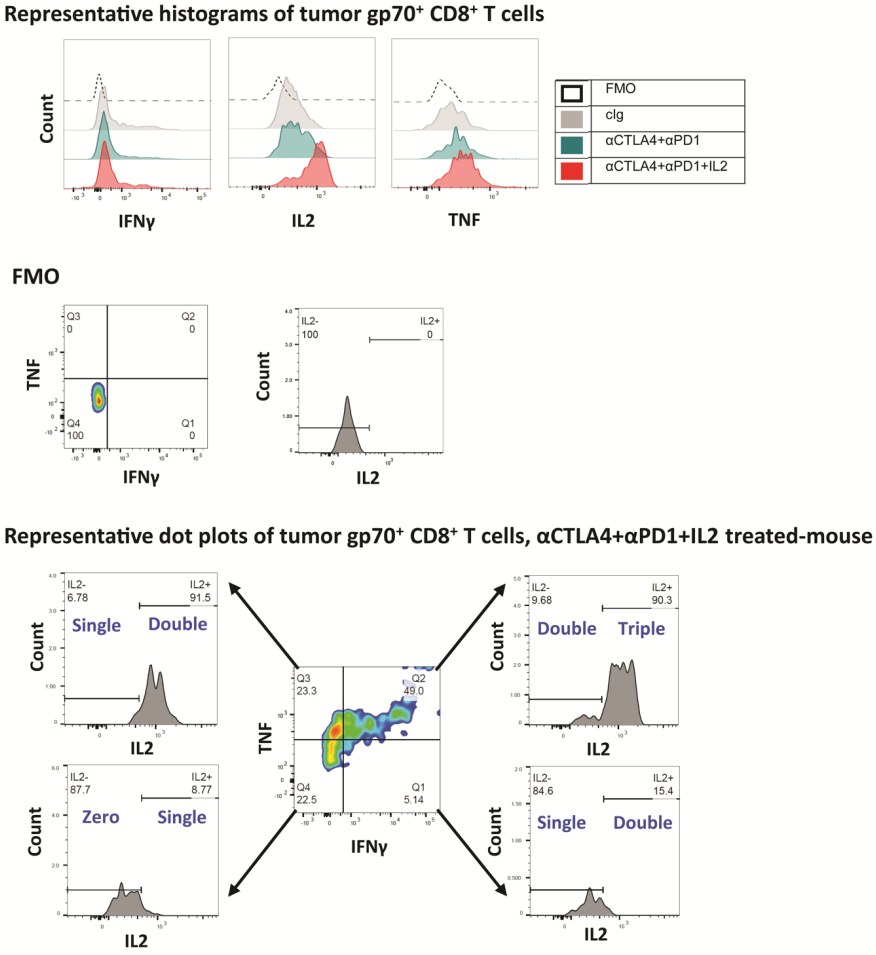

Figure S8. Gating strategy for cytokines⁺ T cells and examples with tumor gp70⁻ and gp70⁺ CD8⁺ T cells expression. From the same experiments as described in Fig. 5. (Upper panel) The same gating strategy as in Fig. S4 was followed for the gating of gp70⁺ CD8⁺ T cells. The gating of cytokines⁺ T cells was based on a FMO samples. Representative overlaid histograms showing the expression of IFNγ, TNF and IL2 in gp70⁺ CD8⁺ TILs. TILs single cell suspension were incubated with monensin and brefeldin A for 5 hour in vitro prior to intracellular cytokine staining. (Lower panel) Representative dot plots are from a sample treated with triple combination and show the gating strategy used to extract frequency of gp70⁺ CD8⁺ T cells expressing zero, one, two, or three cytokines (of IFNγ, TNF and IL2).

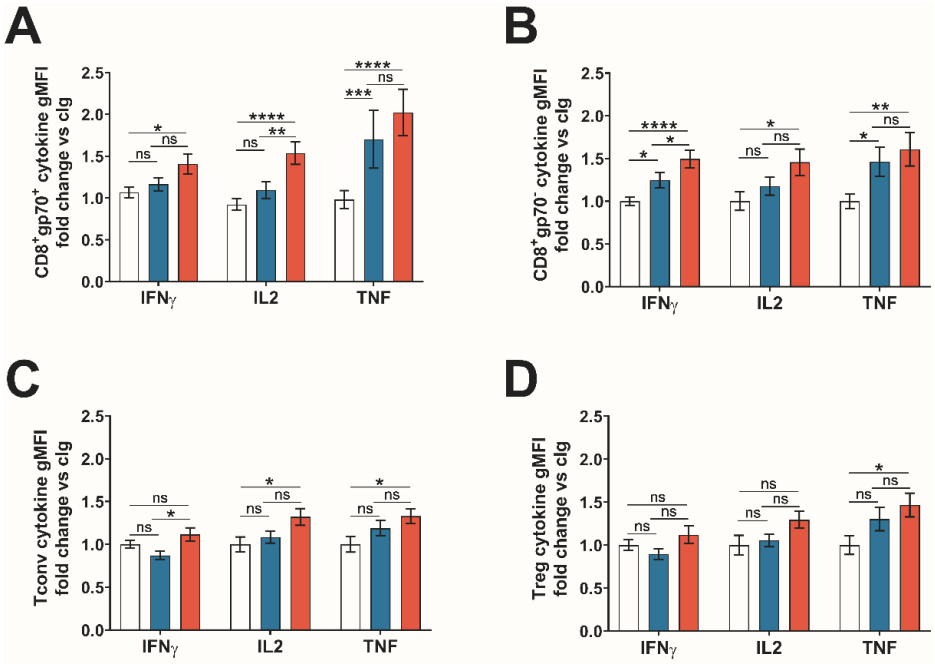

Figure S9. Addition of IL2 to neoadjuvant anti-CTLA4+anti-PD1 increase cytokine expression in CD8⁺ T cells and CD4⁺ Tconv cells. (A to **D)** From the same experiment as described in Fig. 5, tumors from the indicated groups were harvested at day 13 and single cell suspensions generated for flow cytometric analysis. Bar plots showing the fold change of the indicated cytokine gMFI normalized against the mean of clg treated group in **(A)** $CD8^+gp70^+$, **(B)** $CD8^+gp70^-$, **(C)** $CD4^+FOXP3^-$ Tconv, and **(D)** $CD4^+FOXP3^+$ Treg cells (mean±SEM). Data pooled from 3 independent experiments performed and analyzed double-blinded (n=17-23/group). Significant differences between the indicated groups were determined by 2-way-ANOVA with Tukey's multiple comparisons test. * P <0.05, ** P <0.01, ***P<0.001, **** P <0.0001.

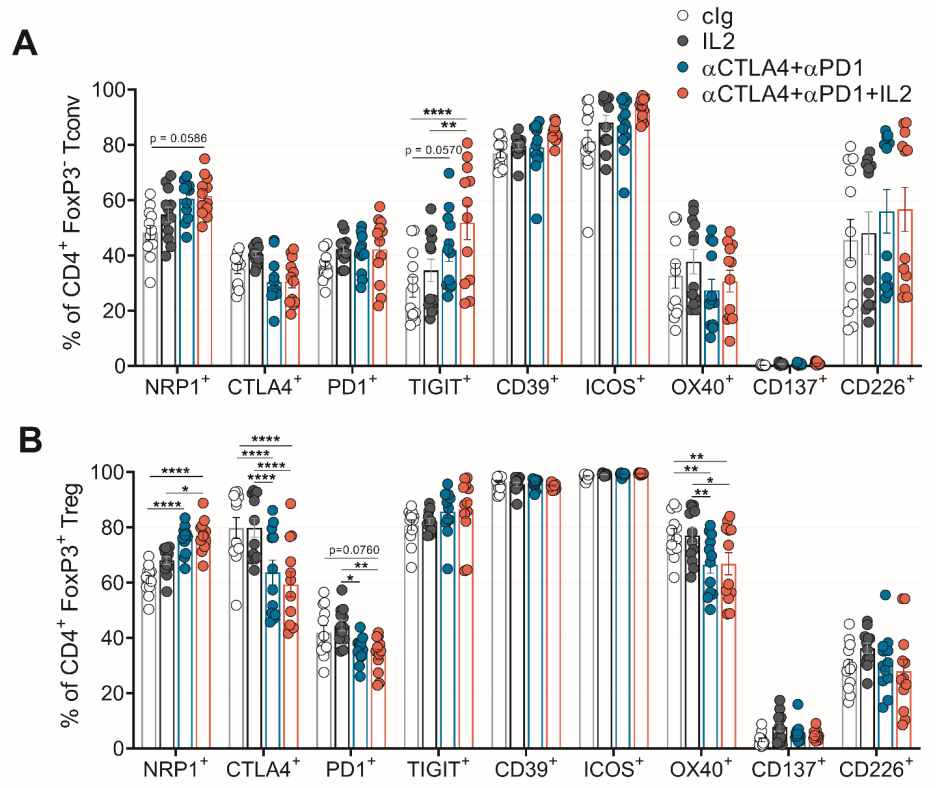

Figure S10. Addition of IL2 to neoadjuvant anti-CTLA4+anti-PD1 does not change Treg and Tconv surface markers expression compared to anti-CTLA4+anti-PD1 alone. (A and **B)** Groups of BALB/c wild type (WT) mice were injected in the 5th mammary fat pad with 4T1.2 tumor cells and treated i.p on days 8 and 10 with the indicated combination of anti-CTLA4, anti-PD1, IL2 or cIg. At day 13, tumors were harvested and single cell suspensions generated for flow cytometry analysis. Proportion of inhibitory (NRP1, CTLA4, PD1, TIGIT, CD39) or co-stimulatory (ICOS, OX40, CD137, CD226) receptors expressed by **(A)** Treg (CD4$^+$FoxP3$^+$) or **(B)** Tconv (CD4$^+$FoxP3$^-$) cells (mean±SEM). Data pooled from 2 independent experiments performed and analyzed double-blinded (n=12/group). Significant differences between the indicated groups were determined by 2-way ANOVA with Tukey's multiple comparisons test, * P <0.05, ** P <0.01, *** P <0.001, **** P < 0.0001.

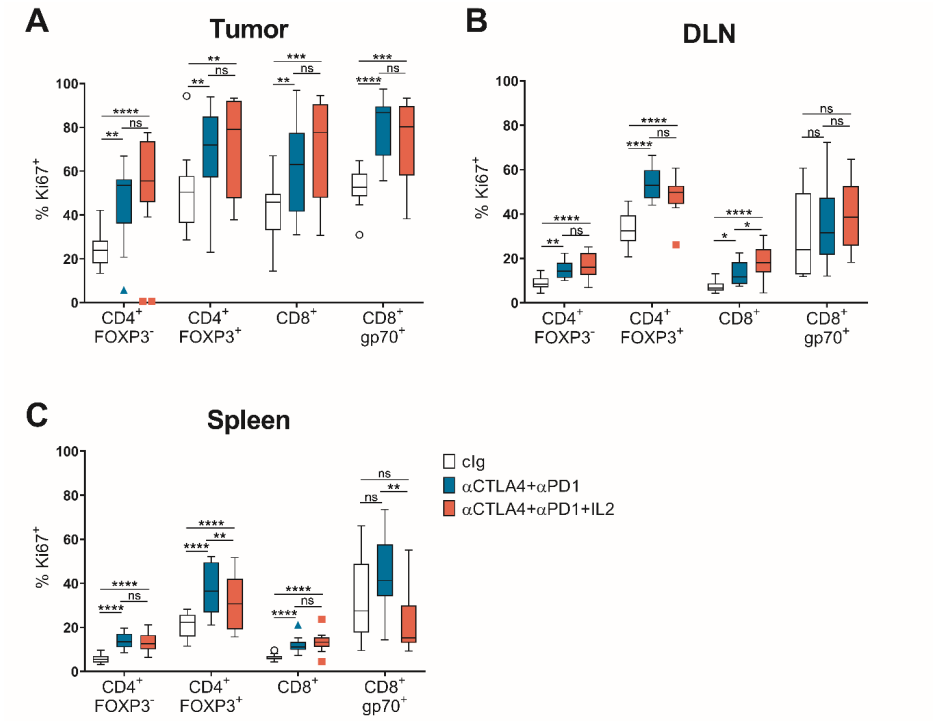

Figure S11. Addition of IL2 to neoadjuvant anti-CTLA4+anti-PD1 immunotherapy increased T cell proliferation. From the same experiment as described in Fig. 5, box plots with Tukey whiskers showing proportion of Ki67$^+$ expressing cells in the indicated T cell subset after treatment in the **(A)** tumor, **(B)** draining lymph node (DLN) and **(C)** spleen. Data pooled from 2 independent experiments performed and analyzed double-blinded (n=9-15/group). Statistical comparisons between groups were performed by 2-way ANOVA with Tukey's correction, *P<0.05, **P<0.01, ***P<0.001, ****P< 0.0001.

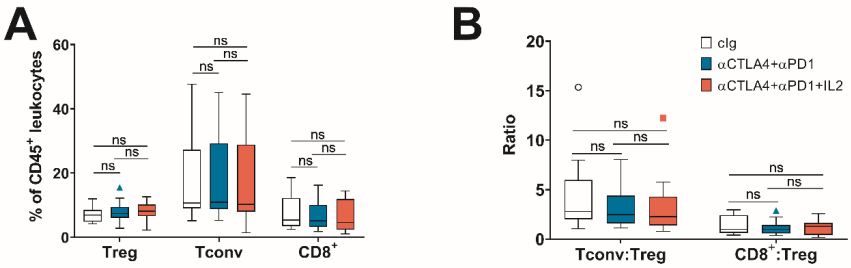

Figure S12. Proportions and ratios of T cell subsets in 4T1.2 tumors following neoadjuvant immunotherapy or cIg. (A and **B)** From the same experiment as described in Fig. 5, tumors from the indicated groups were harvested at day 13 and single cell suspensions generated for flow cytometric analysis. Box plot with Tukey whiskers showing the **(A)** proportions of Tregs (CD4$^+$ FOXP3$^+$), Tconv (CD4$^+$ FOXP3$^-$), and CD8$^+$ T cells and **(B)** ratio of Tconv:Treg and CD8$^+$:Treg. Data pooled from 3

independent experiments performed and analyzed double-blinded (*n*=22-23/group). Statistical comparisons between groups were performed by 2-way ANOVA with Tukey's correction.

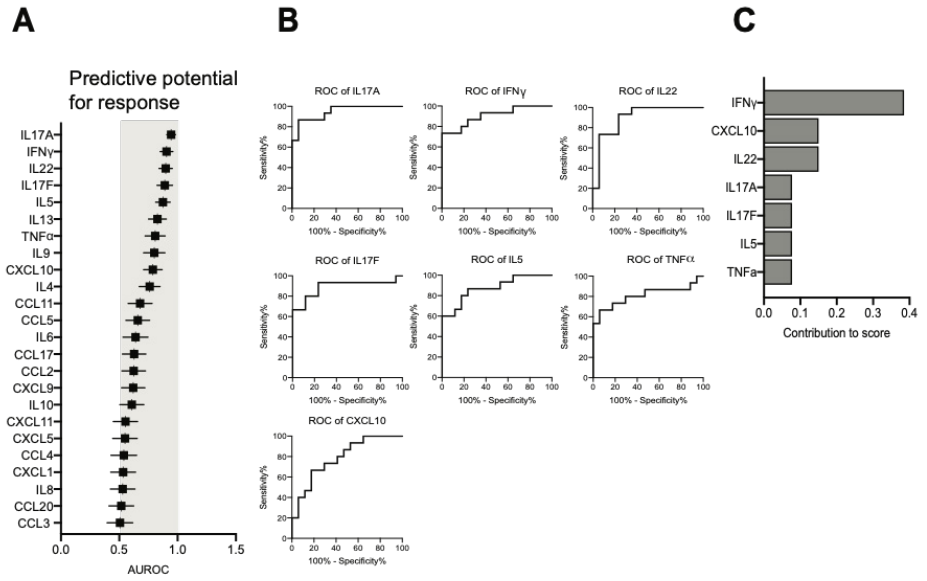

Figure S13. Development of a response score to distinguish responders and non-responders to anti-CTLA4+anti-PD1+IL2 based on the tumor resection cohort. Related to Fig. 3. **(A)** Areas under the ROC curve for distinguishing anti-CTLA4+anti-PD1±IL2 NR from anti-CTLA4+anti-PD1 R and anti-CTLA4+anti-PD1+IL2 R of all 24 soluble chemokine and cytokines. **(B)** ROC curves of soluble markers contributing to the response score. **(C)** Relative contribution of each parameter to the response score.

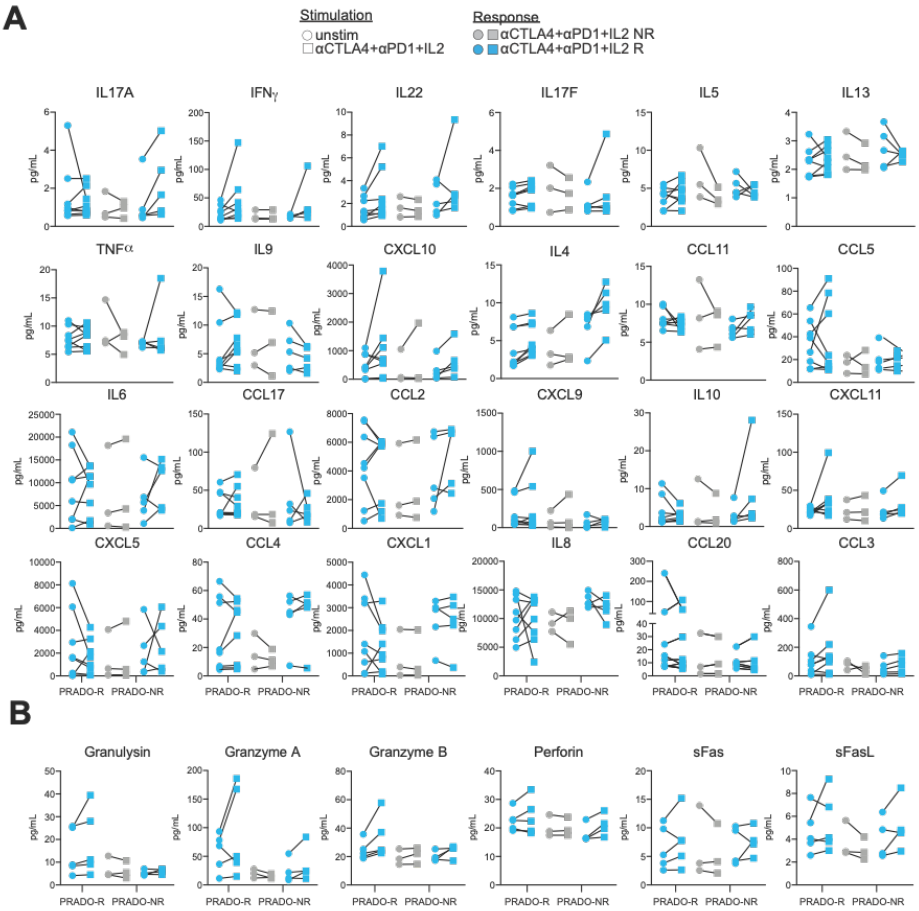

Figure S14. Soluble markers secreted by PDTFs from the melanoma biopsy cohort upon ex vivo treatment. Related to Fig. 6. **(A** and **B)** Parameters related to proinflammatory cytokines and chemokines **(A)** or cytotoxicity **(B)** assessed in untreated and anti(α)CTLA4+αPD1+IL2 treated PDTFs from the PRADO cohort. Parameters are displayed separately for responders (R) to αCTLA4+αPD1 and non-responders (NR) and responders (R) to αCTLA4+αPD1+IL2.